

The effect of metal enrichment and galactic winds on galaxy formation in cosmological zoom simulations

Michaela Hirschmann^{1*}, Thorsten Naab², Romeel Davé^{3,4}, Benjamin D. Oppenheimer⁵, Jeremiah P. Ostriker^{6,7}, Rachel S. Somerville⁸, Ludwig Oser^{2,7}, Reinhard Genzel⁹, Linda J. Tacconi⁹, Natascha M. Förster-Schreiber⁹, Andreas Burkert^{9,10}, Shy Genel¹¹

¹*INAF - Astronomical Observatory of Trieste, via G.B. Tiepolo 11, I-34143 Trieste, Italy*

²*Max-Planck-Institut für Astrophysik, Karl-Schwarzschild Strasse 1, D-85740 Garching, Germany*

³*Astronomy Department, University of Arizona, Tucson, AZ 85721, USA*

⁴*South African Astronomical Observatories, Observatory, Cape Town 7925, South Africa*

⁵*Leiden Observatory, Leiden University, PO Box 9513, 2300 RA Leiden, the Netherlands*

⁶*Department of Astrophysical Sciences, Princeton University, Princeton, NJ 08544, USA*

⁷*Department of Astronomy, Columbia University, New York, NY 10027, USA*

⁸*Department of Physics and Astronomy, Rutgers University, 136 Frelinghuysen Rd, Piscataway, NJ 08854, USA*

⁹*Max-Planck-Institut für extraterrestrische Physik (MPE), Giessenbachstr. 1, 85748 Garching, Germany*

¹⁰*Universitäts Sternwarte München, Scheinerstr.1, D-81679 München, Germany*

¹¹*Harvard-Smithsonian Center for Astrophysics, 60 Garden Street, Cambridge, MA 02138, USA*

Accepted ????. Received ??? in original form ???

ABSTRACT

We investigate the differential effects of metal cooling and galactic stellar winds on the cosmological formation of individual galaxies with three sets of cosmological, hydrodynamical zoom simulations of 45 halos in the mass range $10^{11} < M_{\text{halo}} < 10^{13} M_{\odot}$. Models including both galactic winds and metal cooling (i) suppress early star formation at $z \gtrsim 1$ and predict reasonable star formation histories for galaxies in present day halos of $\lesssim 10^{12} M_{\odot}$, (ii) produce galaxies with high cold gas fractions (30 - 60 per cent) at high redshift, (iii) significantly reduce the galaxy formation efficiencies for halos ($M_{\text{halo}} \lesssim 10^{12} M_{\odot}$) at all redshifts in overall good agreement with recent observational data and constraints from abundance matching, (iv) result in high-redshift galaxies with reduced circular velocities in agreement with the observed Tully-Fisher relation at $z \sim 2$ and (v) significantly increase the sizes of low-mass galaxies ($M_{\text{stellar}} \lesssim 3 \times 10^{10} M_{\odot}$) at high redshift resulting in a weak size evolution – a trend in agreement with observations. However, the low redshift ($z < 0.5$) star formation rates of massive galaxies are higher than observed (up to ten times). No tested model predicts the observed size evolution for low-mass and high-mass galaxies simultaneously. Without winds the sizes of low-mass galaxies evolve to rapidly, with winds the size evolution of massive galaxies is too weak. Due to the delayed onset of star formation in the wind models, the metal enrichment of gas and stars is delayed and agrees well with observational constraints. Metal cooling and stellar winds are both found to increase the ratio of in situ formed to accreted stars - the relative importance of dissipative vs. dissipationless assembly. For halo masses below $\sim 10^{12} M_{\odot}$, this is mainly caused by less stellar accretion and compares well to predictions from semi-analytical models, but differs from abundance matching models as the in situ formed fractions of stellar mass are still too low in the simulations. For higher masses, however, the fraction of in situ stars is over-predicted due to the unrealistically high star formation rates at low redshifts.

Key words: methods: numerical - galaxies: formation - galaxies: evolution - galaxies: stellar content - galaxies: kinematics and dynamics - galaxies: abundances

1 INTRODUCTION

Simple models for galaxy formation assume that gas gets trapped in potential wells of dark matter halos, cools and condenses in central disc, forms stars and self-enriches with a critical galactic stellar mass of the order of $10^{12}M_{\odot}$ so that halos with masses $\gg 10^{13}M_{\odot}$ fragment into many galaxies (e.g. Rees & Ostriker 1977; White & Rees 1978). In hierarchical structure formation scenarios, these processes are accompanied by merger events and continuous gas inflow. However, unaltered inflow and cooling of gas would grossly over-estimate the star formation within a galaxy and result in too massive galaxies known as the 'over-cooling' problem (e.g. White & Frenk 1991; Balogh et al. 2001).

It is plausible that additional 'feedback' processes regulate galaxy growth, i.e. galactic winds driven by supernova explosions or radiation pressure from young massive stars (e.g. Martin 2005; Rupke et al. 2005; Murray et al. 2005). A number of different numerical models for stellar feedback have been developed and implemented in simulations (e.g. Dalla Vecchia & Schaye 2012; Stinson et al. 2012; Davé et al. 2011; Hopkins et al. 2011; Governato et al. 2010; Schaye et al. 2010; Dalla Vecchia & Schaye 2008; Oppenheimer & Davé 2006 and references therein) partly resulting in much better agreement of the galaxy properties with observational constraints. Especially for massive galaxies, energy-driven and/or momentum-driven feedback from accretion onto a central black hole can additionally alter galaxy formation and alleviate the over-cooling problem (e.g. Croton et al. 2006; Somerville et al. 2008; Hopkins et al. 2005; Springel et al. 2005; Ciotti et al. 2010; Teyssier et al. 2011; Puchwein & Springel 2012; Martizzi et al. 2012; Choi et al. 2012; Barai et al. 2013). Overall, such feedback processes are expected to impact the evolution of the stellar galaxy masses, their metal and gaseous content, the efficiency of converting baryons into stars and, as a consequence, also the stellar mass assembly (in situ star formation vs. accretion of stars) and the size evolution (Khochfar & Silk 2006; De Lucia et al. 2006; Naab et al. 2007, 2009; Oser et al. 2010; Hirschmann et al. 2012; Porter et al. 2012; Oser et al. 2012; Hilz et al. 2012; McCarthy et al. 2012; Lackner et al. 2012; Hilz et al. 2013).

Also at higher redshifts observations have now revealed tight correlations between stellar mass, gas mass, star formation rate and metal content like the relation between stellar mass and star formation rate (SFRs), often termed the 'main sequence for star-forming galaxies' (Noeske et al. 2007; Daddi et al. 2007; Elbaz et al. 2007; Genzel et al. 2010). Another example is the relation of stellar mass with gas-phase metallicity (Tremonti et al. 2004; Maiolino et al. 2008; Andrews & Martini 2012). Even though the total gas content of a galaxy is difficult to measure (because atomic, molecular and ionized phases must be accounted for), there are strong indications for galaxies with higher stellar masses to have lower gas fractions (Saintonge et al. 2011; Peeples & Shankar 2011). In general, all these relations evolve with redshift and any successful theoretical framework has to account for this evolution (Tremonti et al. 2004; Gallazzi et al. 2005; Thomas et al. 2005; Erb et al. 2006; Elbaz et al. 2007; Daddi et al. 2007; Salim et al. 2007; Maiolino et al. 2008; Tacconi et al. 2010; Peeples & Shankar 2011; Tacconi et al. 2013; Andrews & Martini 2012).

Despite of the progress in numerical modelling of galaxy formation, the detailed physics of star formation and feedback processes cannot be directly simulated on the relevant small scales but is incorporated in an approximate fashion on sub-resolution scales - more or less motivated by the physics of star formation and observed phenomenology. It has been shown that models driving galactic winds, which can be powered by stellar winds and UV photons from young stars and supernova explosions, can greatly improve the agreement of simulations with observations (Kauffmann et al. 1993; Springel & Hernquist 2003; De Lucia et al. 2004; Oppenheimer & Davé 2006; Stinson et al. 2006; Governato et al. 2007; Oppenheimer & Davé 2008; Murante et al. 2010; Governato et al. 2010; Cen & Chisari 2011; Wiersma et al. 2011; Genel et al. 2012; Barai et al. 2013; McCarthy et al. 2012; Haas et al. 2012; Governato et al. 2012; Hopkins et al. 2012; Kannan et al. 2012; Agertz et al. 2013; Stinson et al. 2013; Aumer et al. 2013; Hopkins et al. 2013; Anglés-Alcázar et al. 2013). Such outflows are now directly observed in most star-forming galaxies up to $z \sim 3$ (Martin 2005; Rupke et al. 2005; Weiner et al. 2009; Steidel et al. 2010; Genzel et al. 2011; Newman et al. 2012). Energy and/or momentum injection from massive stars can be modelled in many different ways into the numerical schemes of simulations. Pure thermal supernova feedback, just heating the surrounding gas, is inefficient (e.g. Katz et al. 1992; Steinmetz & Muller 1995; Katz et al. 1996; Hummels & Bryan 2012) as the dense star-forming gas has a high cooling-rate and the energy can be radiated away very quickly before it can be deposited into the ISM driving a wind (see, however, for a recent improvement Dalla Vecchia & Schaye 2012). This is mainly a result of low resolution: thermal feedback works well at high enough resolution (better than 10 pc, see e.g. Ceverino & Klypin 2009). To overcome this problem (for simulation with not high-enough resolution), energy injection from star-bursts and/or supernovae has been modelled in many different ways: in a kinetic form (e.g. Navarro & White 1993; Cen & Ostriker 2000; Springel & Hernquist 2003; Oppenheimer & Davé 2006; Dalla Vecchia & Schaye 2008), by turning off radiative cooling temporarily (e.g. Stinson et al. 2006; Governato et al. 2007, 2010; Piontek & Steinmetz 2011; Stinson et al. 2013) or by forcing energy injection into the hot and cold gas phase separately (e.g. Scannapieco et al. 2006; Murante et al. 2010).

In this paper, we use a phenomenological feedback scheme presented by Oppenheimer & Davé (2006, 2008); Finlator & Davé (2008); Oppenheimer et al. (2009); Davé (2009); Oppenheimer et al. (2010) and Davé et al. (2011) who implemented scalings expected for momentum-driven winds (Murray et al. 2005; Zhang & Thompson 2012) in large scale cosmological simulations with a typical spatial resolution of a few kpc. It is assumed that the gas outflow rate (i.e. the mass loading) is *inversely* proportional to the stellar velocity dispersion, suppressing star formation in smaller systems, and that the wind velocity is *directly* proportional to the velocity dispersion of a galaxy. With such a scaling for driving winds, high outflow rates and frequent gas re-accretion can be generated leading to a continuous cycle of baryons between galaxies and their surrounding intergalactic medium (IGM) and this cycle is found to impact

ID	NoMW				MNoW				MW			
	M_{vir}	R_{vir}	M_{stellar}	M_{gas}	M_{vir}	R_{vir}	M_{stellar}	M_{gas}	M_{vir}	R_{vir}	M_{stellar}	M_{gas}
0163	966.8	310	28.14	0.793	914.6	305	35.81	0.559	904.7	304	36.58	0.645
0190	699.2	279	27.32	0.840	685.6	277	31.35	0.578	657.7	273	31.92	1.04
0209	699.5	279	18.34	0.462	678.6	276	20.74	0.342	681.3	276	19.67	0.780
0215	668.7	274	25.48	0.521	659.2	273	28.20	0.420	662.1	274	26.92	0.671
0224	654.2	272	20.32	0.419	621.4	268	22.52	0.414	640.3	271	24.56	0.656
0227	705.9	279	27.22	0.848	700.0	279	30.33	0.455	695.4	278	30.90	0.680
0259	592.6	264	17.38	0.451	525.2	253	19.95	0.353	555.2	258	17.80	0.618
0290	570.0	260	18.27	0.548	544.4	256	20.03	0.398	546.7	257	20.65	0.780
0300	498.9	249	17.58	0.550	495.1	248	17.98	0.456	504.4	250	17.01	0.877
0305	453.6	241	12.56	0.428	463.9	243	14.69	0.355	465.6	243	20.37	0.623
0329	466.5	243	17.55	0.689	450.4	241	20.74	0.351	462.0	243	19.98	1.38
0380	443.3	239	14.37	0.617	441.5	239	17.09	0.615	442.4	239	14.99	0.480
0408	332.5	217	13.77	1.502	338.0	219	15.62	0.382	326.7	216	15.69	0.294
0443	362.9	224	17.23	1.082	371.0	226	18.54	0.455	381.1	228	17.46	0.705
0501	306.1	212	14.79	0.408	306.3	212	13.93	0.216	304.6	211	14.79	0.575
0549	281.4	206	10.50	0.404	276.6	205	10.60	0.328	292.7	208	10.58	0.396
0616	260.8	201	12.93	0.442	257.3	200	13.18	0.287	261.3	201	13.37	0.790
0664	208.5	186	8.719	0.236	241.8	196	9.801	0.305	245.8	197	10.0	0.553
0721	194.2	182	10.56	0.220	192.1	181	12.04	0.220	196.0	182	10.77	0.720
0858	188.6	180	10.30	0.397	186.0	179	11.43	0.225	189.1	180	10.93	0.212
0908	172.1	175	9.245	0.506	169.7	174	9.883	0.197	169.4	174	9.077	0.514
0948	162.7	171	6.314	0.146	160.6	171	9.241	0.174	164.8	172	8.471	0.571
0959	158.0	170	6.015	0.157	155.5	169	10.10	0.237	161.1	171	9.379	0.315
0977	139.6	163	2.743	0.273	125.6	157	4.964	0.486	131.4	160	2.774	1.25
1017	139.7	163	6.988	0.182	140.5	163	8.181	0.195	141.8	164	6.453	0.862
1061	139.3	163	6.840	0.191	137.7	162	7.609	0.411	141.4	164	7.375	0.672
1071	146.5	165	8.451	0.185	142.9	164	9.028	0.155	148.3	166	10.27	0.470
1091	147.0	166	8.195	0.256	143.4	164	9.187	0.245	149.1	166	8.006	0.180
1167	127.6	158	7.873	0.451	125.3	157	9.025	0.249	124.3	157	7.461	0.176
1192	104.7	148	5.267	0.125	103.2	147	5.727	0.124	112.0	151	5.189	0.257
1196	136.2	161	8.019	0.565	132.3	160	8.973	0.303	132.3	160	7.772	0.256
1646	95.39	143	5.577	0.173	95.22	149	6.290	0.134	93.03	142	6.250	0.401
1859	81.44	293	9.634	0.444	81.37	293	7.507	0.341	81.68	293	7.084	0.344
2283	54.07	119	2.222	0.202	79.67	135	2.398	0.144	82.87	137	2.205	0.439
2665	50.07	119	3.427	0.090	53.89	119	3.799	0.092	56.10	120	3.710	0.148
3431	33.61	144	3.136	0.113	33.72	145	3.262	0.177	33.22	144	2.161	0.962
3852	41.50	109	3.467	0.174	40.64	108	3.571	0.232	21.81	87.7	0.292	0.387
4234	40.50	108	2.591	0.261	39.15	107	2.826	0.231	40.49	108	0.732	0.513
4323	33.65	101	2.592	0.194	34.21	102	2.750	0.204	34.79	102	1.963	0.660
4662	30.40	98.0	2.406	0.139	30.17	97.7	2.288	0.171	31.10	98.7	1.009	0.571
5014	28.05	136	2.837	0.376	28.18	136	2.924	0.542	28.46	137	0.579	0.361
5988	25.07	91.9	2.203	0.193	24.82	91.6	2.222	0.260	25.74	92.7	0.784	0.552
6622	20.82	86.4	1.389	0.258	20.76	86.3	1.340	0.284	43.18	110	0.665	0.252
6782	22.10	88.1	2.225	0.140	22.33	88.4	2.131	0.207	22.93	89.2	0.373	0.315
7748	17.24	81.1	1.686	0.115	17.52	81.6	1.637	0.150	17.51	81.5	0.506	0.490

Table 1. Halo ID, halo virial mass (M_{vir}), virial radius (R_{vir}), stellar mass (M_{stellar}) and gas mass (M_{gas}) of the *central* galaxies for the three models (45 initial conditions each). All masses are in units of $10^{10} h^{-1} M_{\odot}$ and the virial radius in in units of $h^{-1} \text{kpc}$.

many of the observed galaxy and IGM properties. Although most galaxies in these simulations were not resolved sufficiently well, these models were successful in matching a wide range of global observational data of galaxies and their ISM properties, although some significant discrepancies still remain.

In this study, we present three sets of higher resolution, cosmological zoom simulations of 45 individual galaxy halos using a modified version of Gadget2 including a treatment for metal enrichment (SNII, SNIa and AGB stars) and strong momentum-driven winds (as described in detail in Oppenheimer & Davé 2006, 2008). This extends recent studies by Oser et al. (2010, 2012), which our initial condi-

tions are based on, but containing only thermal SN feedback, which is known to have only a weak effect on suppressing star formation (see e.g. Hirschmann et al. 2012). In the three simulation sets, we add metal enrichment/cooling and the wind model separately to investigate the respective impact on the conversion of gas into stars, the in- and outflow rates of gas, the resulting cold gas fractions, star formation rates and the metal content in the stellar and gaseous phase in halos spanning a mass range of $10^{11} < M_{\text{halo}} < 10^{13} M_{\odot}$ (Note that we also analyse the substructure within a halo considering sub-halo masses down to even $10^{10} M_{\odot}$). Additionally, we examine the effect on the bi-modality in the stellar mass assembly, i.e. the contribution of in situ formed and accreted

stars to the overall stellar content and on galaxy scaling relations, e.g. the mass-size relation or the Tully-Fisher relation. Oser et al. (2010) found that massive galaxies form their stars early in time and grow mainly via accretion of stellar systems at later times explaining the observed stellar downsizing for massive galaxies. In addition, we demonstrate in this study that galactic winds are essential to reproduce *the observed stellar downsizing concerning low-mass galaxies*. Overall in this work, we go beyond previous studies (Finlator & Davé 2008; Davé 2009; Davé et al. 2011) by using the same simulation code, i.e. the same SN feedback prescription, but achieving a significantly increased resolution (by about 1-2 orders of magnitude) in gas/dark matter particle mass. This approach is still useful at higher resolution as it allows to test for convergence of the models in predicting different galaxy properties (see e.g. Vogelsberger et al. 2013). Second, our resolution is higher but still not high enough to reliably apply more direct feedback models (e.g. the Gasoline model requires an at least one of order of magnitude better resolution compared to ours) and it is far from having a resolution where physical processes driving winds can be explicitly captured. Third, with higher resolution we can investigate spatial information such as galaxy sizes, the maximum circular velocities or the radial distributions of metallicities (which will be the topic of a follow-up study).

Despite of the recent progress in numerically modelling the hydrodynamics using e.g. a moving mesh algorithm (e.g. Springel 2010; Sijacki et al. 2012; Kereš et al. 2012; Vogelsberger et al. 2013), the implementations for star formation and stellar feedback still dominate the end results of how galaxies form and evolve, rather than the details of the implementation of the hydrodynamics. Scannapieco (2012), for example, have explicitly demonstrated that different numerical techniques typically lead to differences as more gas seems able to cool and become available for star formation in grid-based codes than in SPH. However, they emphasise that this effect is small compared to the variations induced by different feedback prescriptions. In a recent study of Marinacci et al. (2013) they have shown that to simulate “realistic” Milky-Way-like galaxies (e.g. disk-dominated systems with flat rotation curves) using a moving mesh code, also a (new) strong feedback model is necessary. Overall, this justifies the SPH implementation of GADGET2 used in this paper and demonstrates the importance of studying the effect of galactic winds irrespectively of the used numerical implementation.

The paper is organised as follows. Section 2 provides an introduction into our simulation set-up and the construction of the merger trees. In section 3 we discuss the effect of galactic winds and metal cooling on star formation rates, in- and outflow rates, cold gas fractions and the baryon conversion efficiencies. We continue to focus on the bi-modality of star formation (in situ formed versus accreted stellar content) in our different simulation sets in section 4 and on galaxy scaling relations in section 5. In addition, in section 6 we present stellar and gaseous metallicities and ages of our simulated galaxies. A final summary and discussion of this work is given in section 7.

2 HIGH-RESOLUTION SIMULATIONS OF INDIVIDUAL GALAXY HALOS

2.1 Simulation setup

The cosmological zoom simulations presented in this paper are based on the initial conditions described in detail in Oser et al. (2010, 2012). We briefly review the simulation setup here, but refer the reader to the original papers for more details. The dark matter halos for further refinement were selected from a dark matter only N-body simulation with a co-moving periodic box length of $L = 100$ Mpc and 512^3 particles (Moster et al. 2010). We assume a Λ CDM cosmology based on the WMAP3 measurements (see e.g. Spergel et al. 2003) with $\sigma_8 = 0.77$, $\Omega_m = 0.26$, $\Omega_\Lambda = 0.74$, and $h = H_0/(100 \text{ kms}^{-1}) = 0.72$. The simulation was started at $z = 43$ and run to $z = 0$ with a fixed co-moving softening length of $2.52 h^{-1} \text{ kpc}$ and a dark matter particle mass of $M_{\text{DM}} = 2 \times 10^8 M_\odot h^{-1}$. Starting at an expansion factor of $a = 0.06$ we constructed halo catalogues for 94 snapshots until $a = 1$ separated by $\Delta a = 0.01$ in time. From this simulation, we picked 45 halos identified with the halo finder algorithm *FOF* at $z = 0$. To construct the high-resolution initial conditions for the re-simulations, we traced back in time all particles closer than $2 \times r_{200}$ to the centre of the halo in any snapshot and replaced them with dark matter as well as gas particles at higher resolution ($\Omega_b = 0.044$, $\Omega_{\text{DM}} = 0.216$). In the high resolution region the dark matter particles have a mass resolution of $m_{\text{dm}} = 2.5 \cdot 10^7 M_\odot h^{-1}$, which is 8 times higher than in the original simulation, and the gas particle masses are $m_{\text{gas}} = m_{\text{star}} = 4.2 \cdot 10^6 M_\odot h^{-1}$. The co-moving gravitational softening length for the gas and star particles is $400 h^{-1} \text{ pc}$ and $890 h^{-1} \text{ pc}$ for the high-resolution dark matter particles. For two halos, we have also performed simulations with 16 times higher mass resolution than in the original DM-only simulation (see appendix A).

To model the gas component we use the entropy conserving formulation of SPH (GADGET-2, Springel et al. 2005) with the extension of Oppenheimer & Davé (2006, 2008) including a prescription for metal enrichment and momentum-driven winds. This version includes ionisation and heating by a spatially uniform, redshift dependent background radiation according to Haardt & Madau (2001), where re-ionisation takes place at $z \approx 6$ and the radiation field peaks at $z \approx 2 - 3$. Gas particles undergo radiative cooling down to 10^4 K under the assumption of ionisation equilibrium; we account for metal-line cooling using the collisional ionisation equilibrium tables of Sutherland & Dopita (1993). Following Springel & Hernquist (2003), stars are formed from dense gas clouds using a sub-resolution multiphase model which describes condensation and evaporation in the interstellar medium (McKee & Ostriker 1977). We have a density threshold for star formation of $n_{\text{th}} = 0.13 \text{ cm}^{-3}$, which is calculated self-consistently in a way that the equation of state is continuous at the onset of star formation. This value is the same as in the work of Oppenheimer & Davé (2008) and Davé et al. (2011), but lower than in Oser et al. 2010 (who have a value of $n_{\text{th}} = 0.23 \text{ cm}^{-3}$). Besides, we adopt a Chabrier (2003) IMF throughout this study implying a fraction of stars, which results in type II supernovae, of $f_{\text{SN}} = 0.198$ (different to Oser et al. 2010, who assume a Salpeter IMF with

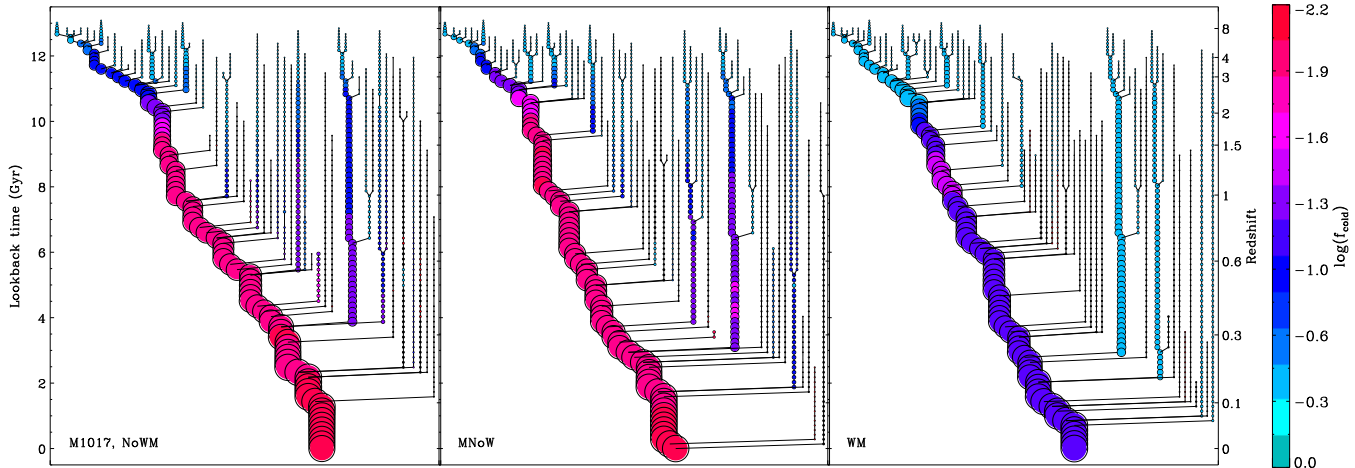


Figure 1. Three merger trees for halo 1017 with a mass of $\approx 10^{12} M_{\odot} h^{-1}$ for a hydrodynamical zoom-simulation without metal enrichment and SN winds (NoWM, left panel), with metal enrichment but no SN winds (MNoW, middle panel) and including both metal enrichment and SN winds (WM, right panel). Black circles indicate the dark matter halos (as identified by the halo finder) and the size of the circles is scaled by the square root of the dark matter virial radius. In addition, the cold gas fractions f_{cold} of the galaxies are colour-coded. The merger trees visualise that simulations including strong winds significantly increase the cold gas fraction (bluer colour).

$f_{\text{SN}} = 0.1$). The model is tuned via a single parameter, the star formation rate timescale, using simulations of isolated disk galaxies to reproduce the observed Schmidt-Kennicutt relation. Note that in cosmological simulations the result may, however, deviate from the observed relation (see Hirschmann et al. 2012).

Following Oppenheimer & Davé (2008), we account for metal enrichment from supernovae type II (SNII), type Ia (SNIa) and asymptotic giant branch (AGB) stars and four elements (C, O, Si, Fe) are tracked individually. The SNII enrichment follows Springel & Hernquist (2003) using an instantaneous recycling approximation, but is modified by adopting metallicity dependent yields from the nucleosynthesis calculations by Limongi & Chieffi (2005). The SNIa rate is modelled following the two-component parametrisation from Scannapieco & Bildsten (2005), where one component is proportional to the stellar mass (slow, delayed component) and the other to the SFRs (rapid component). Besides the production of metals, each SNIa is assumed to deposit 10^{51} ergs of energy, and this energy is added thermally directly to the gas particle. AGB stars mainly provide feedback in form of mass (energy can be neglected as most mass leaves the AGB stars with velocities far below 100 km/s) and produce carbon and oxygen (while silicon and iron remains almost unprocessed). To determine the stellar mass loss rate from non-SN stars as a function of age and metallicity we use the Bruzual & Charlot (2003) stellar synthesis models and interpolate in age and metallicity.

The momentum-driven wind model is based on the wind model of Springel & Hernquist (2003): outflows are directly tied to the star formation rates using the relation $\dot{M}_{\text{wind}} = \eta \dot{M}_{\text{SF}}$, where η is defined as the mass loading factor. Star forming gas particles get stochastically kicked vertically to the disc and are thus, launched in a wind with the probability η . A selected wind particle is given the additional velocity of v_w in the direction of $\mathbf{v} \times \mathbf{a}$, where \mathbf{v} and \mathbf{a} are the velocity and acceleration of a particle, respectively

(Springel & Hernquist 2003). Subsequently, the gas particles are decoupled from hydrodynamics for a short time in order to escape their dense, star-forming regions and eventually to leave their galaxies (see e.g. Dalla Vecchia & Schaye 2008). These particles are only allowed to again interact hydrodynamically as soon as they either reach a SPH density less than 10 per cent of the SF density threshold or the time it takes to travel 30 kpc at the wind velocity v_w (note that the first case significantly exceeds the instances of the second case). The values of η and v_w define the wind model: while Springel & Hernquist (2003) used constant values for these parameters, Oppenheimer & Davé (2006) adopt a momentum-driven wind model and introduce a scaling with the velocity dispersion of the galaxies motivated by observations of galactic super-winds of Martin (2005); Rupke et al. (2005) and by analytical calculations of Murray et al. (2005); Zhang & Thompson (2012). The magnitude of the kick is given by

$$v_w = \sigma(2.9 + 4.29\sqrt{f_L - 1}), \quad (1)$$

where f_L is the luminosity factor (critical luminosity in terms of Eddington luminosity to expel gas out of the galaxy). f_L is randomly selected from $f_L = [1.05 - 2]$ for each particle following the observations by Rupke et al. (2005) and is dependent on metallicity due to a higher UV photon output from lower metallicity stellar populations

$$f_L = f_{L,\odot} \times 10^{-0.0029 \times (\log Z + 9)^{2.5} + 0.4177}. \quad (2)$$

The mass-loading factor η (i.e. the fraction of star-forming particles, which get kicked) is calculated according to

$$\frac{\dot{M}_w}{\text{SFR}} = \eta = \frac{\sigma_0}{\sigma}, \quad (3)$$

where $\sigma \propto M_{\text{gal}}^{1/3}$ is the velocity dispersion which is calculated from the galaxy mass using an on-the-fly group finder. σ_0 is a constant which is set to reproduce the overall evolution of the SFR density in Oppenheimer & Davé (2006)

(here: $\sigma_0 = 300$ km/s). For low resolution simulations of large cosmological boxes this empirical model was shown to reproduce the observed metal enrichment of the intergalactic medium at $2 < z < 5$ (Oppenheimer & Davé 2006), the mass metallicity relation (Finlator & Davé 2008), the cold gas fractions (Davé et al. 2011), the SFRs (Davé et al. 2011) and baryon conversion efficiencies (Davé 2009) at various redshifts. This model is clearly empirical and phenomenological. However, the implemented scalings are consistent with observations and analytical estimates for momentum-driven winds. This model captures the effect of the wind but not its origin on unresolved scales. In this sense it might be as valuable as many other sub-resolution models. The model itself regulates how much gas is expelled from a galaxy with a given SFR and mass. The mass loading regulates the delayed formation of galaxies (the star formation histories, see section 3.1) what might therefore be considered as a model input. Other galaxy properties, like the size evolution or the fractions of in situ to accreted stellar mass, the evolution of the mass-metallicity relation can be considered as model predictions.

To disentangle the effects of metal enrichment and galactic winds we study the influence on galaxy properties separately by running the full set of simulations with three different models:

- **NoWM**: No metal enrichment (only gas cooling for a primordial composition of hydrogen and helium) and no galactic winds (only thermal energy injection due to SNII explosions), comparable to the results of Oser et al. (2010), Oser et al. (2012) and Hirschmann et al. (2012).
- **MNoW**: Metal enrichment and metal cooling, but no galactic winds
- **WM**: Metal enrichment and momentum-driven galactic winds

Table 1 summarises global properties (halo mass, virial radius, stellar mass and gas mass) of the 135 re-simulations. Note that all simulations include thermal supernova feedback as described in detail in Springel & Hernquist (2003)¹. For our analysis, we will not only consider the central galaxy within the re-simulated halo, but also the corresponding satellite galaxies with halo masses above $10^{10} M_\odot$ within the virial radius of the parent halo at $z = 0$. The halo masses of satellites are determined at the time of their accretion onto their final parent halos. Including satellite galaxies in our analysis extends our galaxy sample towards lower masses which are stronger affected by the wind feedback.

2.2 Merger trees

We extract the merger trees for the dark matter component directly from the cosmological re-simulations as described in Hirschmann et al. (2010). For every snapshot at a given redshift, we first identify individual dark matter haloes using a FOF (Friends-of-Friends) algorithm with a linking length of $b = 0.2$ (Davis et al. 1985). In a second step we extract the sub-halos of every FOF group using the SUBFIND algorithm

(Springel et al. 2001). This halo finder identifies over-dense regions and removes gravitationally unbound particles. In this way we split the FOF group into a main or host halo and its satellite halos. In most cases, 90% of the total mass is located in the main halo.

The sizes and virial masses of the main halos (i.e. the most massive SUBFIND halos) are determined by a spherical over-density criterion. The minimum halo mass is set to 20 particles ($5 \times 10^8 M_\odot/h$). The mass of a central object is defined by the dark matter mass within the virial radius using the over-density approximation in the spherical collapse model according to Bryan & Norman (1998). The algorithm to connect the dark matter halos between the snapshots at different redshifts is described in detail in Maulbetsch et al. (2007). The branches of the trees for $z = 0$ halos are constructed by connecting the halos to their most massive progenitors (MMP) at previous snapshots. Thereby, halo j with n_j particles at redshift z_j with the maximum probability $p(i, j)$ is chosen to be a MMP of halo i containing n_i particles at redshift z_i (where $z_j < z_i$). The probability $p(i, j)$ is defined as

$$p(i, j) = \frac{n_{ov}(i, j)}{n_{max}(i, j)} \quad \text{with} \quad (4)$$

$$n_{ov} = n_i(z_i) \cap n_j(z_j) \quad \text{and}$$

$$n_{max}(i, j) = \max(n_i(z_i), n_j(z_j))$$

Here, n_{ov} is the number of particles found in both halos and n_{max} is the particle number of the larger halo. We remove ‘fake’ haloes which exist only within one time step and have no connection to any branch (halo masses are generally near to the resolution limit). The low redshift ends of the branches are then checked for mergers. A halo j at t_j is assumed to merge into halo i at t_i , if at least 50% of the particles of halo j are found in halo i . In case of a merger the branches are connected.

Note that the tree-algorithm is only applied to the dark matter particles – star or gas particles are not separately traced back in time. They are assumed to follow the evolution of the dark matter. Therefore, we assign to each dark matter halo in a tree a hot/cold phase gas mass by counting hot/cold gas particles within the virial radius of the central halo. The stellar and cold gas particles within 1/10 of the virial radius ($:= r_{10}$) are defined as the stellar and gas mass of the central galaxy. We distinguish between hot and cold gas particles by using the following definition:

$$\log T < 0.3 \log \rho + 3.2 \rightarrow \text{cold} \quad (5)$$

$$\log T > 0.3 \log \rho + 3.2 \rightarrow \text{hot}, \quad (6)$$

where T is the temperature and ρ is the density divided by the mean baryon density. Note that the above discrimination between hot and cold gas was established by looking directly at the phase diagrams of the re-simulations, where we have divided between the gas in the disk heated by SN feedback and the shock heated gas. With the above definition for cold gas we mainly capture the dense, star-forming gas.

In Fig. 1 we visualise three merger trees of the same re-simulated halo with a virial mass of $1 \times 10^{12} M_\odot$ (M1071) for the three different simulation sets. The size of the black circles approximates the dark matter halo mass as they scale with the square root of mass normalised to the final dark matter halo mass. The cold gas fractions ($= M_{\text{cold}}/(M_{\text{cold}} +$

¹ A certain fraction of formed stars is expected to explode immediately as supernovae which heat the surrounding gas with an energy input of 10^{51} ergs.

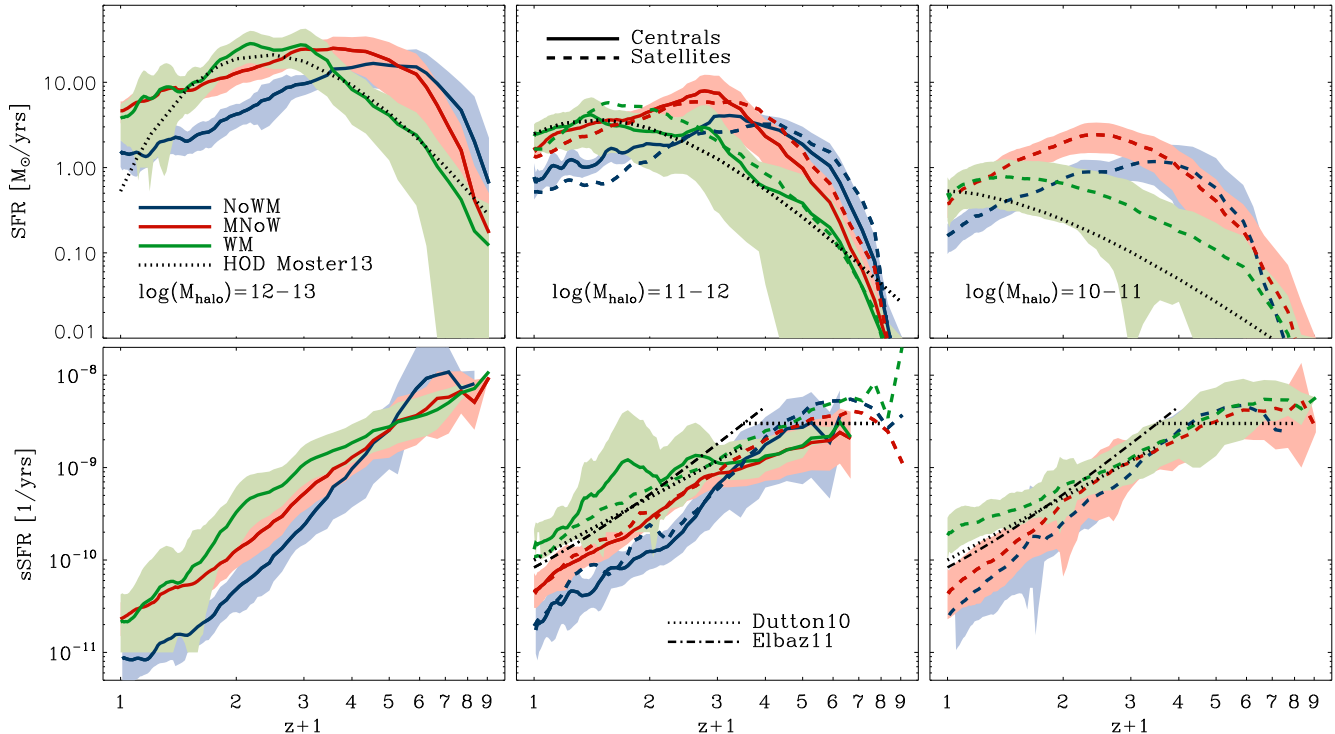


Figure 2. Top row: Mean star formation rates (SFR) versus redshift ($z+1$) for the three models (blue: NoWM, red: MNoW, green: WM) in three different halo mass bins (different columns, considering the *present-day* halo masses). Centrals are illustrated by solid, satellites by dashed lines. The coloured areas indicate the $1\text{-}\sigma$ scatter of the mean SFRs. The early star formation on the WM runs is efficiently by galactic winds and is in reasonable agreement with SHAM predictions (Moster et al. 2013, black dotted lines) for halo masses above $10^{11} M_{\odot}$. Bottom row: Same as in the top row, but for the mean specific star formation rates (sSFR’s). The WM runs can reproduce the decline of the observed sSFR’s (of star-forming galaxies) with redshift: $\propto (z+1)^{2.25}$ for galaxy masses between $10^9 - 10^{11} M_{\odot}$ (illustrated by black dashed lines, see observational compilation of Dutton et al. 2010; Reddy et al. 2012) and the one found by Elbaz et al. (2011) (black dotted-dashed lines).

M_{stellar}) of the galaxies residing in the dark matter halos are colour-coded (as indicated by the colour bar). In all three models, galaxies at high redshift contain a larger cold gas content, which either turns into stars or is heated towards lower redshifts. However, simulations including strong winds (WM) reveal a significantly larger cold gas fraction than the simulations without winds, at all redshifts.

3 CONVERSION OF GAS INTO STARS

An important and useful parameter describing galaxy formation is the efficiency with which gas is turned into stars. This efficiency might vary with time and redshift and is influenced by gas outflows which not only determine the cold gas mass and the stellar content in a galaxy but also influence ‘secondary’ galaxy properties such as the metal content, the stellar mass assembly, i.e. the relative contributions from in situ star formation and accretion of stars, and as a consequence the structural evolution of galaxies over cosmic time.

3.1 Star formation rates

We start by investigating the star formation rates (SFRs) of our simulated galaxies within $r_{10} := 1/10 \times r_{\text{vir}}$ (for the

satellites we use r_{10} of their own sub-halo), shown in the top row of Fig. 2. We consider in our analysis both central (solid lines) and satellite galaxies (dashed lines) in the three different simulation sets (green: WM; red: MNoW; black: NoWM). We have binned the centrals and satellites into overall three halo mass bins: $12 < \log M_{\text{gal}}/M_{\odot} < 13$ & $11 < \log M_{\text{gal}}/M_{\odot} < 12$ for centrals and $11 < \log M_{\text{gal}}/M_{\odot} < 12$ & $10 < \log M_{\text{gal}}/M_{\odot} < 11$ for satellites (different panels) and averaged over the SFRs in each mass bin.

The NoWM runs show significant early star formation: for the most massive halos, the SFRs peak at $z \sim 5$ and are decreasing towards lower redshifts (top left panel). With decreasing halo mass, the peaks of the SFRs are slightly moved towards lower redshifts (e.g. $z \sim 3$ for halos with $10 < \log M_{\text{gal}}/M_{\odot} < 11$, bottom right panel), illustrating a mild trend of stellar downsizing or anti-hierarchical stellar evolution. According to Neistein et al. (2006) this a ‘‘natural’’ consequence of CDM models. For the MNoW runs, the peak of star formation is slightly shifted towards lower redshifts ($z = 2 - 4$ depending on the halo mass bin), again followed by a decline. The shift of the peak is due to a higher star formation in a larger number of small halos as a consequence of more efficient cooling (in low-mass halos). In other words, gas cools and turns into stars preferentially in smaller halos rather than falling into larger ones at high redshifts

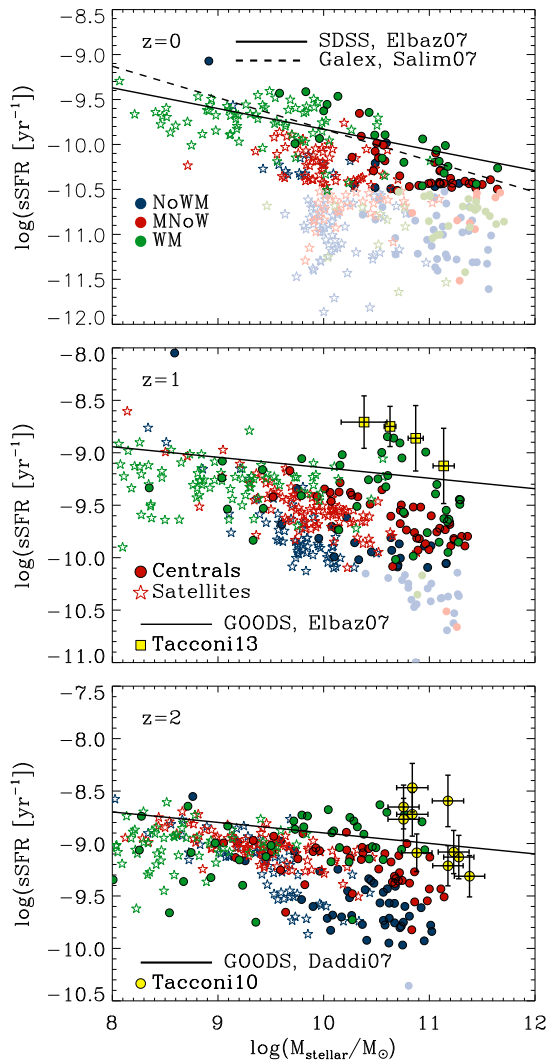


Figure 3. $sSFR$'s versus galaxy masses at $z=0,1,2$ (top, middle, and bottom panel) for the three models for *star-forming* central/satellite galaxies (with $sSFR > 0.3/t_{\text{Hubble}}$, bright circles/stars) and *quiescent* central/satellite galaxies (with $sSFR < 0.3/t_{\text{Hubble}}$, light circles/stars), respectively. The simulation results are compared to the observed star-forming sequence of galaxies from SDSS and GOODS (black solid lines, Elbaz et al. 2007; Daddi et al. 2007) and to recent observational data from Tacconi et al. (2010) and Tacconi & et al. (2013) (yellow symbols). MW runs reproduce the observed relation fairly well at all redshifts.

(and thus, delaying the peak of the SFR in larger galaxies). Simulations with wind feedback (WM runs) reveal a more moderate increase of star formation at high redshifts. For the high and intermediate mass bins, star formation peaks between $z = 1 - 2$, while for the low mass bin, the SFR peaks below $z = 0.5$. Therefore, the WM model predicts a much more pronounced trend of stellar downsizing than the NoWM model: low mass galaxies form at significantly later times than their corresponding (low-mass) host halos which - in a cold dark matter dominated universe preferentially form at early times (White & Frenk 1991). The early formation of low mass galaxies in the WM runs is suppressed

due to the efficient ejection of star forming gas (see equation 3), particularly in low mass galaxies and also at high redshifts (as here the re-infall rate is still low in contrast to low redshifts where recycled gas accretion becomes the dominant source of gas infall for new star formation, see e.g. Oppenheimer & Davé 2006; Oppenheimer et al. 2010).

The time evolution of the SFRs is compared to predictions from the sub-halo abundance matching (SHAM) model as presented in Moster et al. (2013) (dotted black lines in the top row of Fig. 2). Note that we have used the average halo mass in each mass bin as an input value for the SHAM fitting functions. For halo masses above $10^{11} M_{\odot}$, we find a good agreement between the WM simulations and the SHAM model. Only at low redshifts (below $z = 1$) the WM runs predict higher SFRs for massive galaxies compared to the SHAM model as too much gas is cooling and forming stars. This implies that in massive galaxies a further mechanism might be needed to efficiently suppress star formation as e.g. feedback from accreting black holes (Croton et al. 2006; Sijacki et al. 2007; Somerville et al. 2008; Puchwein et al. 2008; Booth & Schaye 2009; Fabjan et al. 2010; McCarthy et al. 2010; van de Voort et al. 2011; Fanidakis et al. 2011; Bower et al. 2012; Hirschmann et al. 2012; Dubois et al. 2013; Puchwein & Springel 2013).

Turning to the lowest halo mass bin (top right panel), even the SFRs in the WM simulations are slightly higher than the SHAM predictions for the whole redshift range, although low-mass satellites match the observed SFR - stellar mass relation well, as we will discuss later in Fig. 3. This indicates that these low mass halos contain too massive galaxies (see also baryon conversion efficiencies in Fig. 7). This over-production of stars at early times in halos with masses between $10^{10} - 10^{11} M_{\odot}$ is also consistent with over-producing the mass of these galaxies at $z = 0$. A solution for this problem would be to assume a higher mass-loading for low mass halos. For example, a recent study of Davé et al. (2013) has demonstrated that an energy-driven wind model for dwarf galaxies (mass loading scaling with σ^{-2}) can reduce the amount low-mass galaxies and thus, match the low-mass end of the stellar mass function better. Nevertheless to summarise, the overall evolution of the peaks of the SFRs with halo mass (i.e. the stellar downsizing) as predicted by the SHAM method is quantitatively very well captured by the WM model.

In the bottom row of Fig. 2, we show the evolution of the specific star formation rates $sSFR = SFR/M_{\text{stellar}}$. Overall, the $sSFR$'s are continuously decreasing towards low redshifts. The WM model shows the slowest decrease, in particular for galaxies in lower mass halos. This is in good agreement with observations presented by Dutton et al. (2010); Elbaz et al. (2011) and Reddy et al. (2012) indicating that $sSFR$'s $\propto (z+1)^{2.25}$ below $z = 2.5$ and flat $sSFR$'s at higher redshifts.

In Fig. 3 we show the $sSFR$'s of the three different models as a function of galaxy stellar mass at $z = 0, 1, 2$ (from top to bottom) in comparison to observations. The solid and dashed black lines indicate observational results from different surveys (SDSS & GOODS & GaleX; Elbaz et al. 2007; Daddi et al. 2007; Salim et al. 2007) and the yellow symbols illustrate the observational results from recent studies by Tacconi et al. (2010) and Tacconi & et al. (2013). Here we

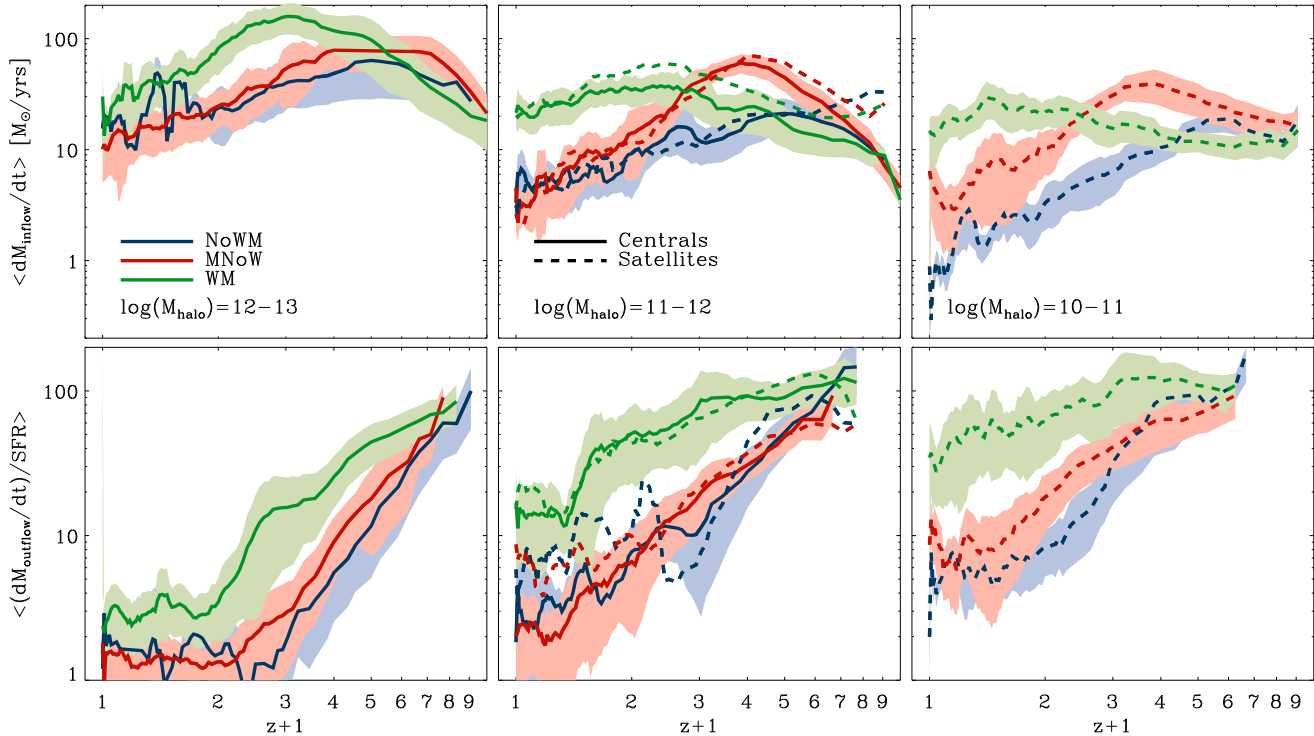


Figure 4. Cosmic evolution of the inflow rates (top row) and the mass loading factors ($= \langle \dot{M}_{\text{outflow}}/SFR \rangle$, bottom row) for different halo mass bins (different columns) and distinguishing between centrals and satellites (solid and dashed lines, respectively). Different colors illustrate the NoWM (blue), the MNoW (red) and the WM (green) simulation runs. The lines indicate the mean value, while the corresponding shaded areas show the $1\text{-}\sigma$ scatter. In general, at $z \lesssim 3-4$, galactic winds increase the gas inflow (and outflow) rates and thus, lead to high mass loading factors.

have separated the simulated galaxies into quiescent (light green, red and blue symbols) and star-forming (dark green, red and blue symbols) using the Franx et al. (2008) definition: galaxies are quiescent for $\text{sSFR} < 0.3/t_{\text{Hubble}}$. While the NoWM and MNoW runs in general under-predict the sSFR's of star-forming galaxies at a given stellar mass, the sSFR's in the WM simulations are in reasonably good agreement with the observed trend although the absolute SFRs (at least for massive systems) seem to be too high. This is in qualitative agreement with Davé et al. (2011) who find that (for large cosmological boxes) the WM model significantly over-estimates the number density of galaxies at the massive end of the stellar mass function ($M_{\text{gal}} \geq 10^{11} M_{\odot}$) and also the high end of the SFR distribution function. They attribute this failure to a missing mechanism to efficiently suppress star formation in *massive* galaxies (e.g. feedback from AGN) primarily at low redshift. However, for lower mass galaxies ($M_{\text{gal}} < 5 \times 10^{10} M_{\odot}$), we obtain slightly higher sSFR's at low redshifts than the previous results of Davé et al. (2011), a possible effect of the higher resolution (i.e. increasing star formation with increasing resolution, see Appendix A).

3.2 Inflow, outflow and mass loading of gas

To explicitly demonstrate the influence of the galactic winds and fountains on the balance of gas inflow and outflow we present in Fig. 4 the cosmic evolution of the mean gas inflow

rates (top row), and of the 'mass-loading' factors (bottom row) for star forming centrals and satellites in different halo mass bins. We consider the flows through a sphere with radius r_{10} . The 'mass-loading' is then computed as

$$\left\langle \frac{\dot{M}_{\text{outflow}}}{SFR} \right\rangle, \quad (7)$$

where \dot{M}_{outflow} is the outflow rate. Note that the evolution of the outflow rates is not shown explicitly but their behaviour follows the one of the inflow rates.

We find that at high redshifts ($\gtrsim 3-4$) the inflow (and outflow) rates in the models without winds are higher than in the WM model. This most likely reflects the inflows (and outflows) of hot gas which appear in a hydrostatic equilibrium (of a hot halo) in the models without winds. The early emergence of a hot halo is a consequence of the earlier assembly of stellar structures in the NoWM and the MNoW models than in the WM model and of the resulting gravitational energy release from in-falling stellar systems (i.e. gravitational feedback, see Johansson et al. 2009 and Naab et al. 2007). In contrast, at redshifts below $\lesssim 3$, the inflow (and outflow) rates in the WM model are always larger than in the models without galactic winds. The high outflow rates are a direct consequence of expelling the star-forming gas in the wind model, while the high inflow rates reflect the accretion of recycled gas, which has been blown out at earlier times and which is according to Oppenheimer et al. (2010) the dominant mode of gas accretion since $z = 1.5$ (besides

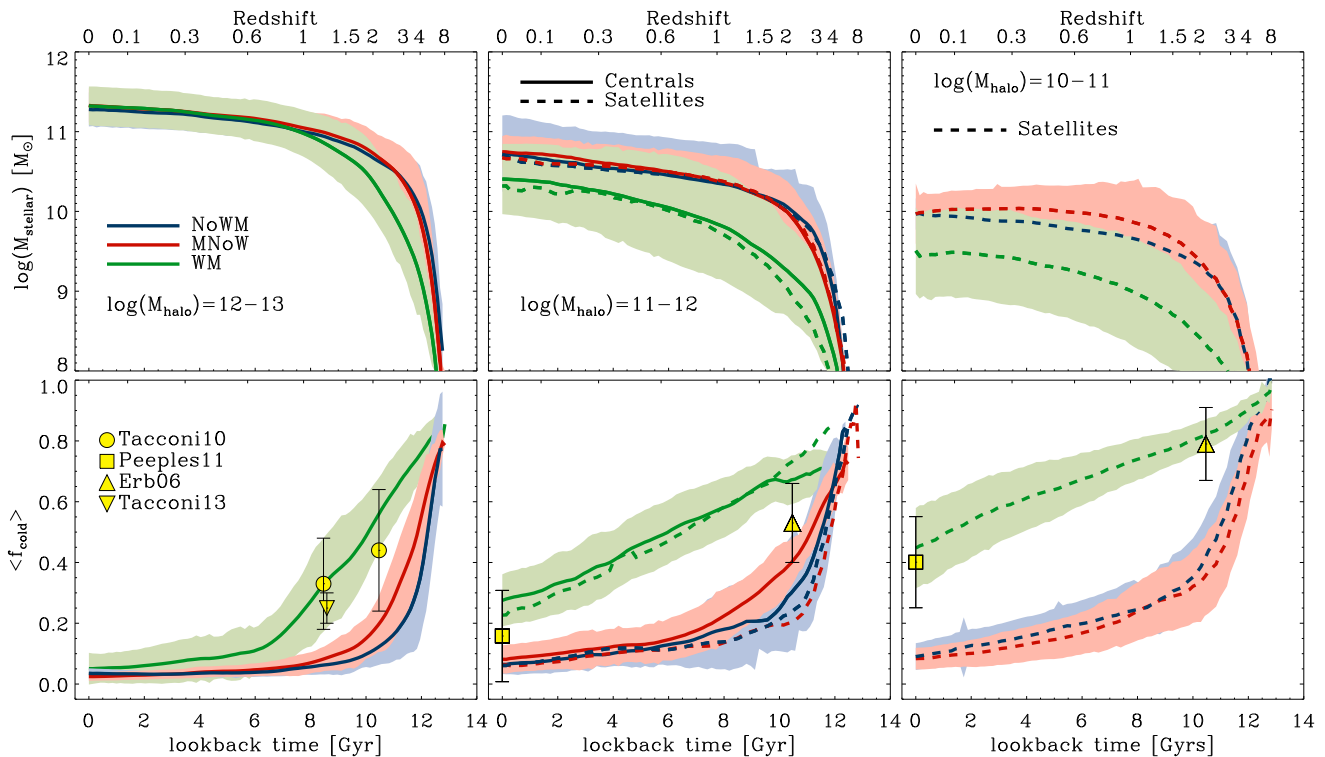


Figure 5. Time evolution of the average stellar mass (top row) and the average cold gas fractions (bottom row) of the simulated galaxies in different halo mass bins (different columns) separated by centrals (solid lines) and satellites (dashed lines). Different colours correspond to the three NoWM (blue), MNoW (red) and WM (green) models. The shaded areas show the $1\text{-}\sigma$ scatter of the mean values. Runs including momentum-driven winds lead to significantly higher cold gas fractions, particularly in low mass galaxies, which are in reasonably good agreement with observational data (yellow symbols, Erb et al. 2006; Tacconi et al. 2010; Peebles & Shankar 2011; Tacconi & et al. 2013).

cold and hot mode accretion). In the highest halo mass bin (left top panel) the inflow (and outflow) rates in the WM model are strongly declining below $z \sim 2$ and reaching at $z = 0$ similar values as in the NoWM and the MNoW models, whereas in galaxies residing in halos with masses below $10^{11} M_{\odot}$, the inflow (and outflow) rates remain almost constant below $z \sim 2$ and are at $z = 0$ by roughly an order of magnitude higher than in the models without any galactic winds.

Turning now to the mass loading factors (bottom row in Fig. 4), all models predict a decreasing mass loading with decreasing redshift. At very high redshifts $z > 5$ the mass loading is similarly high in all three simulation runs. With decreasing redshift, however, the mass loading factors in the NoWM and MNoW models exhibit a similarly strong decline, while for the WM model the decline is much shallower and thus, the mass loading factors are always higher than in the models without galactic winds, particularly for low-mass halos. This explicitly demonstrates the efficiency of stellar winds on the strength of mass loading (by definition). Only for the most massive halos the mass loading factors in the WM run at $z = 0$ are found to be similarly low as those in the runs without winds as the galactic wind feedback is less efficient in blowing gas out of massive galaxies at low redshifts and as the SFRs are still high (due to the high re-infall rates of previously ejected gas).

3.3 Cold gas fractions

In Fig. 5 we show the evolution of the stellar mass (top row) and the cold gas fractions (bottom row). The cold gas fraction is computed as

$$f_{\text{cold}} = \frac{M_{\text{cold}}}{M_{\text{cold}} + M_{\text{stellar}}}, \quad (8)$$

where M_{cold} is the cold gas mass and M_{stellar} is the stellar mass within r_{10} . We find a general trend for lower mass galaxies to have higher cold gas fractions. For the NoWM and MNoW runs the evolution of the galaxies is very similar. The cold gas fractions at all masses decrease very rapidly with time so that already by $z \approx 2$ the cold gas fractions are below 20%. Due to very efficient early star formation most of the gas is consumed early-on. Including metal enrichment only slightly increases the cold gas masses (and fractions) due to enhanced cooling. It is notable that in both models the cold gas fractions of the satellites decrease faster than for the centrals at the *same* halo mass. This may be caused by environmental processes like strangulation, ram-pressure stripping etc. working only on satellite galaxies (e.g. Gunn & Gott 1972; Abadi et al. 1999; Quilis et al. 2000; van Gorkom 2004; Roediger & Brüggén 2007; Kawata & Mulchaey 2008; McCarthy et al. 2008; Font et al. 2008; Bekki 2009 and references therein). For the WM runs, the cold gas fraction are significantly higher than for the NoWM and MNoW runs. In

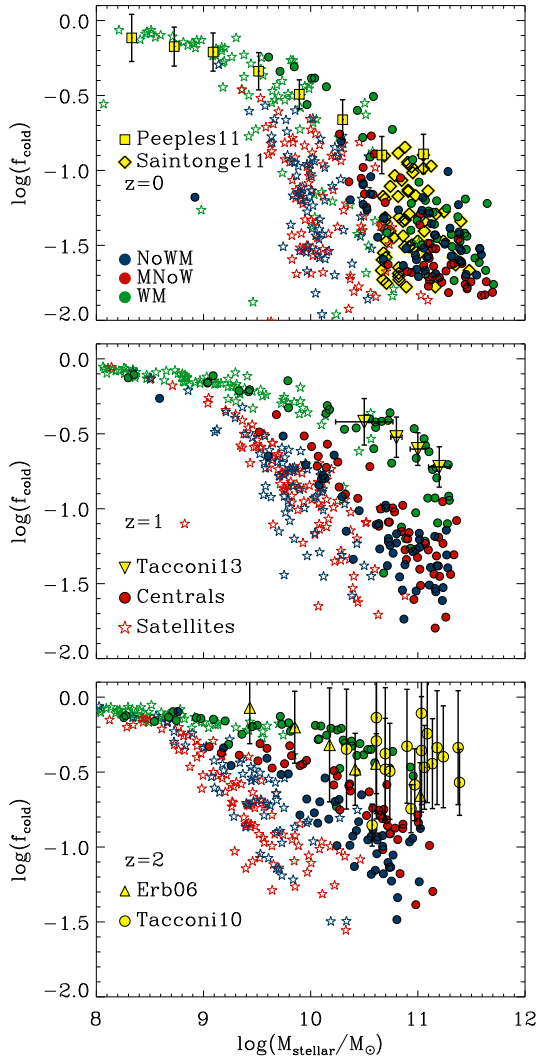


Figure 6. Cold gas fractions versus galaxy masses at $z=0$, 1, 2 (top, middle and bottom panel) for the three models (indicated by different colours). Filled circles indicate central galaxies, while open stars correspond to satellite galaxies. Yellow triangles, squares and circles show observations from Tacconi & et al. (2013); Peebles & Shankar (2011); Tacconi et al. (2010); Erb et al. (2006), respectively. The WM runs including metal cooling and winds can match the observational data at all redshifts fairly well.

particular at $z \approx 2$ the winds result in 4-5 times higher cold gas fractions. This is caused both by *lower stellar* masses (top row of Fig. 5) and at the same time *higher cold gas* masses irrespectively of whether the galaxy is a central or a satellite. At higher redshifts ($z \gtrsim 3$), the cold gas mass in the WM runs tends to be slightly lower than in the models without winds (not explicitly shown), while the stellar masses are significantly lower. Towards lower redshifts, however, we find that the cold gas mass in the WM runs is *always* larger than in the NoWM and MNoW models. There is also a clear trend for lower mass galaxies to have higher gas fractions. This is a consequence of the re-accretion of recycled gas in the WM model (Oppenheimer et al. 2010; Weinmann et al. 2012). The increased cold gas fractions in the WM runs

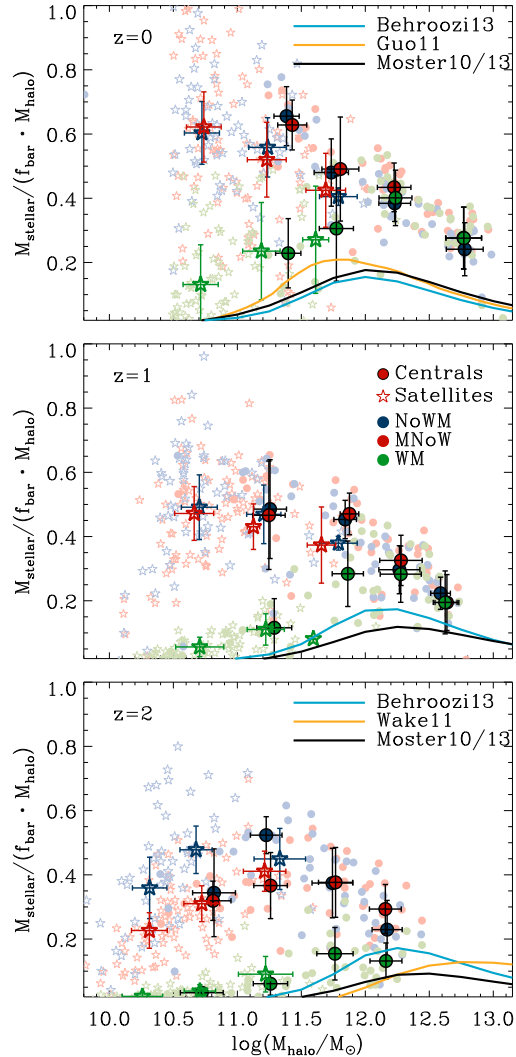


Figure 7. Baryon conversion efficiencies at $z=0$, 1, 2 (top, middle and bottom panel) for the three models (indicated by different colours). Filled circles and open stars indicate central and satellite galaxies, respectively. Solid lines show the predictions from different abundance matching models of Moster et al. (2010); Guo et al. (2011); Wake et al. (2011); Behroozi et al. (2013); Moster et al. (2013). At $z \sim 2$, the WM model matches the predicted conversion efficiencies fairly well at all halo masses. At $z = 0$, all simulation sets predict too high conversion efficiencies, in particular the models without winds (NoWM, MNoW) at low halo masses. The wind model WM accounts for the shape but overall predicts higher galaxy masses by a factor of 2 to 4.

are caused by suppression of early star formation, delaying the conversion of gas into stars towards lower redshifts as galactic winds are very efficient in blowing out star-forming gas particularly for low-mass galaxies which can be re-accreted at later times and thus, leading to an increased amount of cold gas compared to the models without galactic winds (e.g. Oppenheimer & Davé 2006; Stinson et al. 2006; Davé et al. 2011; Stinson et al. 2012, 2013). In general, the gas fractions of the MW model agree much better with observations (here we have not distinguished between molecular and atomic hydrogen). We have indicated respective

observations (Tacconi et al. 2010; Peeples & Shankar 2011; Erb et al. 2006)) by yellow symbols on the bottom panels of Fig. 5.

A more consistent comparison of simulated and observed gas fractions and stellar masses at $z = 0, 1, 2$ is presented in Fig. 6. Filled circles illustrate central, open stars satellite galaxies in simulations. Yellow symbols correspond to different measurements of cold gas fractions as indicated in the legend (Erb et al. 2006; Tacconi et al. 2010; Saintonge et al. 2011 and Tacconi & et al. 2013²) In agreement with previous results (Davé et al. 2011) the NoWM and MNoW runs consistently under-predict observed gas fractions while the empirical wind models are in reasonable agreement with observations at all redshifts and all galaxy masses.

3.4 Baryon conversion efficiencies

Fig. 7 shows the baryon conversion efficiencies versus dark matter halo mass at $z = 0, 1, 2$ compared to results from different abundance matching models (black, light blue and orange lines) of Moster et al. (2010); Guo et al. (2011); Wake et al. (2011) and Behroozi et al. (2013); Moster et al. (2013). The baryon conversion efficiency is defined as:

$$\text{Conversion efficiency} = \frac{M_{\text{stellar}}}{f_{\text{bar}} \cdot M_{\text{halo}}}, \quad (9)$$

where $f_{\text{bar}} \approx 0.17$ is the universal baryon fraction. The lightly colored symbols in Fig. 7 illustrate the individual values for the simulated galaxies, while the full coloured, large symbols show the binned values with a $1-\sigma$ scatter.

At $z = 0$, massive central galaxies are at least two to four times more massive than predictions from abundance matching, independent of the assumed model (see also Oser et al. 2010 and Hirschmann et al. 2012). The origin for the over-production of stars is, however, different. In the NoWM and the MNoW models, too many stars are already formed at high redshift, in particular in low mass halos (see Fig. 2 and middle and bottom panel of Fig. 7). In the WM model, there is too much in situ star formation at redshifts $z \leq 1$ caused by the infall of recycled gas and possibly missing AGN feedback (see Davé 2009). Increasing the mass loading ($\sigma_0 \approx 600 - 900$ km/s) or the kick velocity does slightly lower the present day baryon conversion efficiencies but reduces the SFR at $z > 1$ too much. This indicates that the WM model cannot fully account for processes driving the evolution of galaxies in massive halos ($M_{\text{halo}} > 10^{12} M_{\odot}$). There is only a small difference in the baryon conversion efficiencies of the NoWM and the MNoW models, in contrast to semi-analytic models which normally predict larger differences (Hirschmann et al. 2012). Towards lower masses only the MW runs follow the predicted relation with a comparable constant offset. Using a similar wind model, Davé (2009) find lower baryon conversion efficiencies for present-day, low-mass halos. This can be interpreted as a consequence of their lower spatial resolution (see Appendix A). Both models without winds significantly over-predict the stellar masses at higher redshifts. At $z \approx 2$ the galaxy stellar

masses of the wind model agree with the abundance matching constraints very well both at high and low masses and for satellites and centrals due to the efficient suppression of early star formation (see Fig. 2). The difficulty of predicting low baryon conversion efficiencies in dwarf galaxies and matching observed galaxy abundances was already raised in a previous study by Sawala et al. (2011) who stated that dwarf galaxies formed in their and all other hydrodynamical simulations at that time are more than an order of magnitude more luminous than expected for haloes of this mass. The importance and the success of adopting a strong stellar feedback in simulations to overcome this problem and to regulate the star formation efficiencies over a large range was also demonstrated by other recent studies such as the one of Munshi et al. (2013) using the GASOLINE code with a blastwave supernova feedback.

4 THE TWO MODES OF STELLAR MASS ASSEMBLY

Galaxies can grow their stellar masses in two ways: by converting cold gas into stars in situ in the galaxy or by accreting stars that have formed in other galaxies in mergers (Abadi et al. 2003; Naab et al. 2007; Johansson et al. 2009; Oser et al. 2010). We refer to these two modes as 'in situ' and 'accreted'. The relative amount of in situ and accreted stars was found to vary systematically with galaxy mass in simulations, for semi-analytical models as well as for estimates from abundance matching (Oser et al. 2010; Lackner et al. 2012; Gabor & Davé 2012; Johansson et al. 2012; De Lucia et al. 2006; Guo & White 2008; Hirschmann et al. 2012; Moster et al. 2013; Behroozi et al. 2013; Yang et al. 2013).

In Fig. 8 we show the time evolution of the mass of in situ formed stars (left panels), accreted stars (middle panels) and the ratio of the two (right panels) for three halo mass bins. Note that we have only considered central galaxies here and the halo mass bins have changed with respect to previous figures. The abundance matching results from Moster et al. (2013) are indicated by the black lines. The NoWM galaxies grow rapidly and in situ star formation dominates at high redshift $z > 1$ followed by accretion of stars at $z < 1$. The contribution from accreted stars can dominate the overall mass budget of the most massive galaxies. Already the inclusion of metal cooling reduces the importance of accretion: high-mass galaxies grow faster at high redshifts due to enhanced cooling and the accreted stellar mass is slightly reduced (also because the accreted galaxies are slightly more dominated by gas, see Figs. 5 and 6). However, galactic winds have the most dramatic effect. For all galaxies the amount of accreted stars is significantly reduced as the merging halos host galaxies with significantly higher gas masses and lower stellar masses (see Figs. 5 and 7). As a result, galaxies in halos at $\sim 10^{12} M_{\odot}$ accrete less than 10 percent of their stars. The ratio of in situ formed stars is still high for massive galaxies. Here the galaxies are, however, influenced by the potentially unrealistically high star formation rates. These may be reduced by additional feedback from AGN, compensating the effect of stellar winds and metal cooling (e.g. Croton et al. 2006; Bower et al. 2006; Cattaneo et al. 2006;

² We have used the incompleteness corrected $z \sim 1$ data from the Tacconi & et al. 2013 PHIBSS sample.

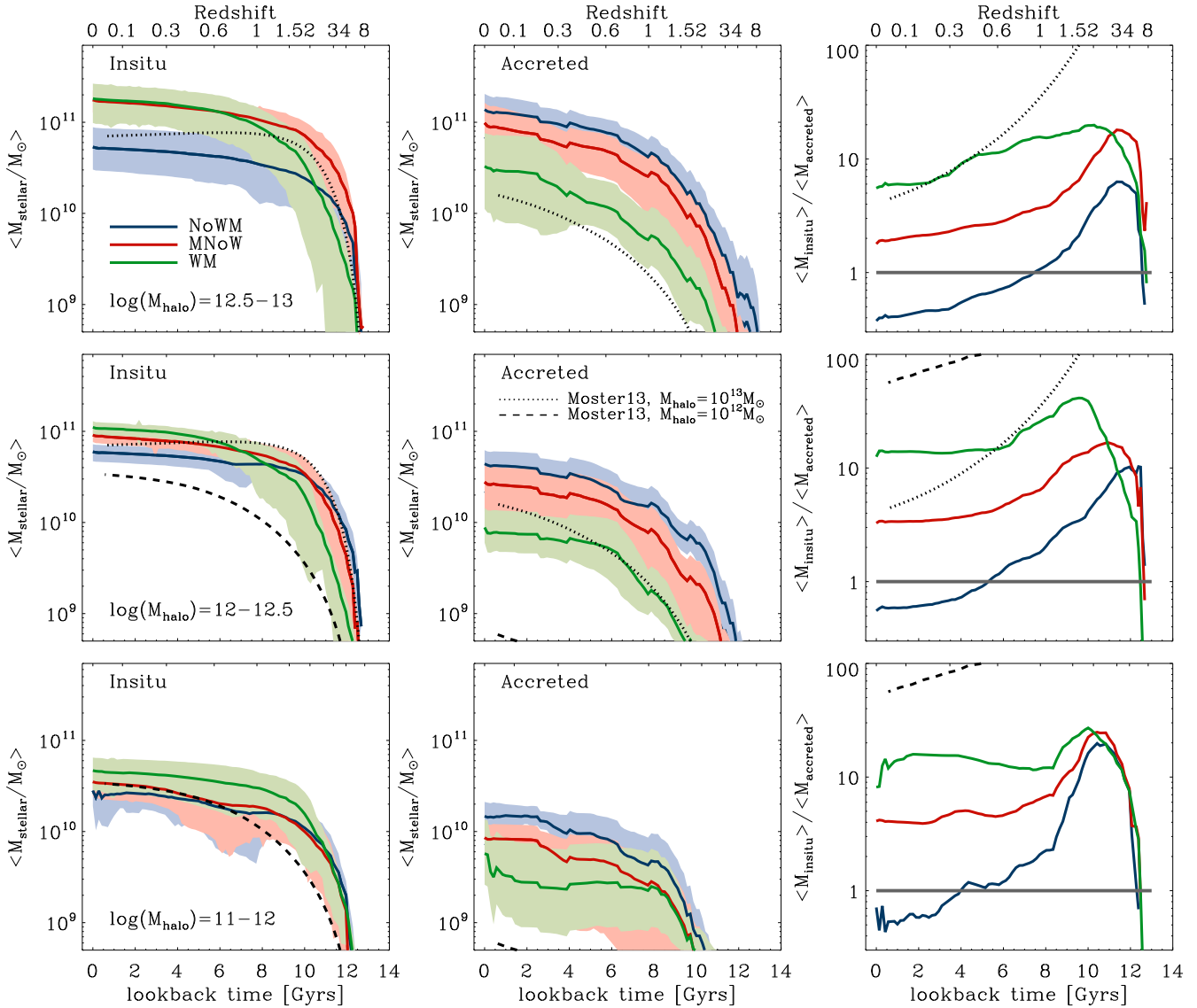


Figure 8. Time evolution of in situ formed stars (left column), accreted stars (middle column) and the fraction of the two (right column) in three different halo mass bins (from top to bottom, considering the *present-day* halo masses). Different models are illustrated by different colours. The solid lines show the average value, while the shaded areas illustrate the $1\text{-}\sigma$ -scatter. Both metal cooling (MNoW) and galactic winds (WM) increase the in situ/accreted ratio due to a smaller amount of accreted stars and a higher in situ star formation than in the NoWM runs. Model results are compared to the predictions from the SHAM approach (Moster et al. 2013, black dashed and dotted lines for $10^{12} M_{\odot}$ - and $10^{13} M_{\odot}$ -mass halos, respectively).

Kang et al. 2006; Monaco et al. 2007; Bower et al. 2008; Somerville et al. 2008). Hirschmann et al. (2012) demonstrated that the fraction of in situ formed to accreted stellar mass is reduced by a factor of ~ 4 in massive galaxies when AGN feedback is considered using semi-analytic models. Recently, Dubois et al. (2013) also indicated with direct simulations that AGN feedback can suppress late in situ star formation leading to a dominance of accretion of stars in massive galaxies with halo masses $4 \times 10^{12} < M_{\text{halo}} < 8 \times 10^{13} M_{\odot}$ (with similar accreted fractions as in Oser et al. 2010). This clearly suggests that feedback from AGN and metal cooling/galactic wind feedback in massive galaxies seem to have *compensating* effects on fraction of accreted stars.

Turning now to the in situ formed fraction of stel-

lar mass, the studies by Moster et al. (2013) and also by Yang et al. (2013) (using the conditional stellar mass function, the CSMF model based on local observational constraints of the star formation rates of central galaxies) find for halo masses of $M_{\text{halo}} \sim 10^{13} M_{\odot}$ present-day, in situ fractions of 80 and 75 per cent, respectively, which is in good agreement with our value of 85 per cent for the WM model (see black dotted and green solid lines in the top right panel of Fig. 8). Instead, our in situ fractions are somewhat too high compared to the results of Behroozi et al. (2013) who apply a similar method as Moster et al. (2013), but obtain lower in situ fractions between 30 and 40 per cent. At halo masses below $M_{\text{halo}} < 3 \times 10^{12} M_{\odot}$, Moster et al. (2013) and Yang et al. (2013) also predict higher, present-day in situ

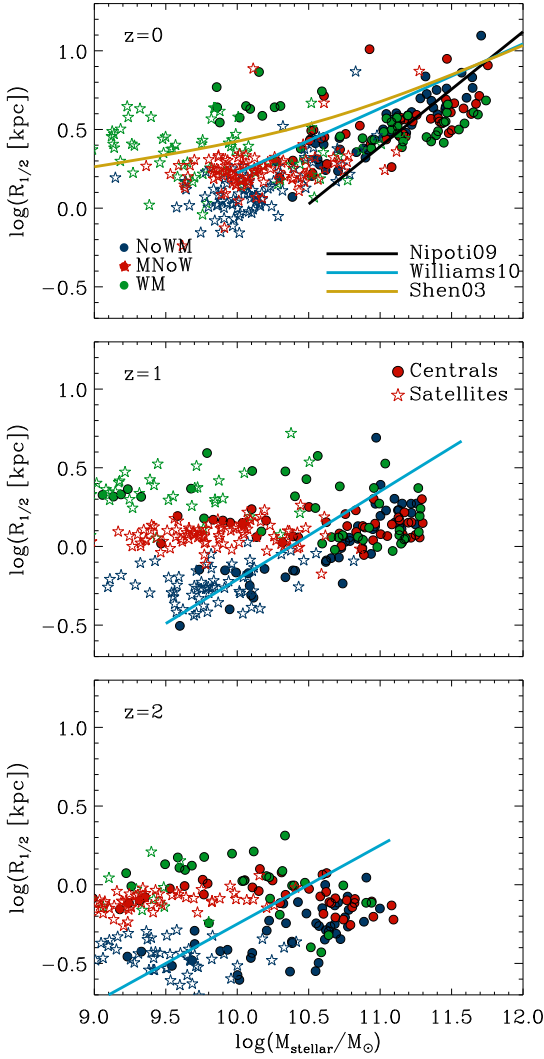


Figure 9. Mass-size relation of central (circles) and satellite galaxies (stars) at $z = 0, 1, 2$ (top, middle and bottom panel) for the three models (indicated by different colours). The half-mass radii have been computed using the projected stellar half-mass radius within r_{10} . Simulation results are compared to two different observed relations for *elliptical* galaxies (Nipoti et al. 2009; Williams et al. 2010) and *spiral* galaxies (Shen et al. 2003). High-mass galaxies are typically smaller using the WM model which over-predicts late in situ star formation, while low-mass galaxies are typically disk-dominated and thus, larger in the WM than in the NoWM model.

fractions between 85 and 99 per cent, in qualitative agreement with the ~ 93 per cent in the WM run, while the results of Behroozi et al. (2013) predict lower in situ fractions of 55 and 80 per cent for 10^{12} - and $10^{11} M_{\odot}$ -mass galaxies, respectively. However, for the lowest halo mass bin the in situ fractions in the WM model are low compared to the SHAM prediction (see green solid and black dashed lines in the bottom right panel of Fig. 8). Overall, this analysis demonstrates that metal cooling and strong winds seem to be necessary and essential to produce high in situ fractions (as derived from observations) in lower mass halos. The significant deviations to the SHAM/CSMF model - which do

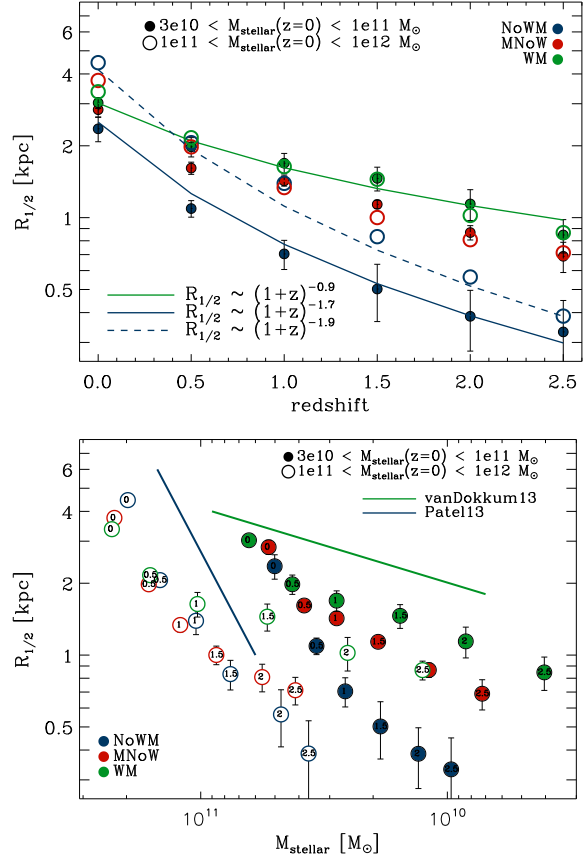


Figure 10. Mean half-mass radii versus redshift (top panel) and versus stellar mass of the progenitor galaxies (bottom panel) considering only central galaxies binned according to their present-day stellar mass (filled circles: $3 \times 10^{10} < M_{\text{stellar}} < 10^{11} M_{\odot}$, open circles: $10^{11} < M_{\text{stellar}} < 10^{12} M_{\odot}$). Different simulation models are shown by different colours. The green and blue, solid and dashed lines in the top panel show a fit to the WM and NoWM models for the two different mass bins. The numbers within the circles in the bottom panel indicate the redshift. The size evolution for one simulation model hardly changes when varying the present-day stellar mass with the consequence that for the massive galaxies, only the NoWM model can capture the strong, observed size evolution (blue solid line in bottom panel, Patel et al. 2013), while the weaker size evolution in the WM model is in rough agreement with the observed slope of intermediate mass galaxies (green solid line in bottom panel, van Dokkum & et al. 2013).

reproduce the cosmic star formation rate history - also indicate the need for an improved treatment of galactic winds (i.e. stronger suppression of early star formation in low-mass halos). A possible, purely observational test for the accreted versus in situ formed stellar fraction are abundance gradients at large radii ($r > r_{\text{eff}}$). Here, the models predict that accreted stars assemble typically at larger radii and originate from lower mass galaxies with lower metallicities. Therefore steep stellar metal gradients - at radii where stars typically do not form - might indicate high accreted fractions. Additional insight might come from the distribution of globular cluster systems (see e.g. Forbes et al. 2011, 2012). Only the wind

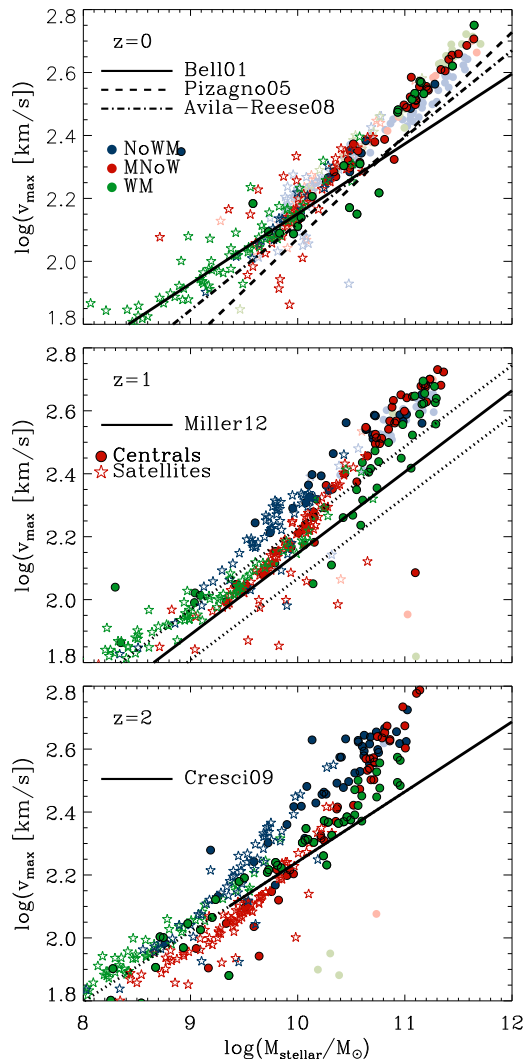


Figure 11. Tully-Fisher relation at $z = 0, 1, 2$ (from top to bottom) for the three models distinguishing between star-forming (full colours) and quiescent galaxies (light colours). Filled circles and open stars indicate central and satellite galaxies, respectively. The maximum rotation velocities have been computed at r_{10} using the contribution from stars, gas and the dark matter halo. Simulation results are compared to observed relations from Bell & de Jong (2001); Miller et al. (2012) and Cresci et al. (2009).

model predicts such steep gradients which we will demonstrate in a follow up study.

Recently, Lackner et al. (2012), who employ an AMR code (ENZO) with metal cooling and thermal supernova feedback (and thus, corresponding to our red curves), predicted a dominance of in situ star formation in massive galaxies for the entire redshift range, in agreement with our MNoW model, but in contrast to Oser et al. (2010) (whose accreted fractions are twice as high). Lackner et al. (2012) attribute these discrepancies to the different modelling of supernova feedback which is more efficient in their simulations. Numerical resolution and assumed star formation efficiencies might play a significant role as well.

5 SCALING RELATIONS

Fig. 9 shows the projected stellar half-mass radius (i.e. the size) versus galaxy mass for central (circles) and satellite (stars) galaxies for the three models at $z = 0, 1$ and 2 (different panels). The half-mass radius of a galaxy is defined as the *projected radius, within which half of the final galaxy mass within r_{10} is included*.

Compared to observations of early-type galaxies by Nipoti et al. (2009) or Williams et al. (2010) (black and blue solid lines), the NoMW model predicts reasonable sizes for massive galaxies ($M_{\text{stellar}} > 10^{11} M_{\odot}$, top panel of Fig. 9), in agreement with Oser et al. (2012). In contrast, massive galaxies in the simulation runs including metal cooling and/or winds (where a larger fraction of the galaxies is star-forming) have sizes which are about ~ 0.2 dex too small compared to the observed most massive galaxies $\log(M_{\text{gal}}/M_{\odot}) > 11.3$. This is most likely a direct consequence of the reduced fraction of accreted stellar mass and the high in situ star formation at all times (see section 4), which significantly suppresses the size growth at low redshifts. This result is in agreement with a recent study of Dubois et al. (2013) who show that simulations without AGN feedback produce too small sizes as a consequence of a high, late in situ star formation. In their work, they attribute AGN feedback to be responsible for a significant growth of the size of a massive galaxy since $z \sim 2$ as a direct result of a significantly increased accretion of stars at late times and a reduction of star formation at the galaxy centre due to the released energy by the AGN. As for the two modes of the stellar mass assembly, this demonstrates clearly (and maybe not surprisingly) the opposite effects of AGN feedback and metal cooling/stellar winds on the size evolution of massive galaxies. Overall, even if the NoWM model can successfully reproduce the mass-size relation as opposed to the WM model, it does not “justify” the NoWM model but instead indicates a missing process in the WM model which is most likely feedback from AGN. However, the most massive galaxies at higher redshifts ($z = 1, 2$ in the middle and bottom panel of Fig. 9), their half-mass radii at a given stellar mass, do not vary much for the different models and even compared to observations from Williams et al. (2010), all of them tend to be very compact.

At present, simulated galaxies in the NoWM and MNoW model with stellar masses of $M_{\text{stellar}} < 5 \times 10^{10} M_{\odot}$ (top panel in Fig. 9) are small compared to the observed mass-size relation for late-type galaxies (beige line, Shen et al. 2003). Instead, galaxies simulated with the WM model have a factor of two to three larger sizes and agree well with the observed sizes. Also at higher redshifts ($z = 1, 2$ middle and bottom panel of Fig. 9), the WM model results in larger low mass galaxies resulting in an interesting turnover at redshift $z = 2$: low mass galaxies are larger than high-mass galaxies. In a study of Brooks et al. (2011) using high-resolved disk simulations performed with GASLINE (including a blastwave feedback scheme), they can also demonstrate that their simulated disks provide an excellent match to the observed magnitude-size relation for both local disks and for disks at $z = 1$.

The increased sizes in the MNoW model (compared to the NoMW model) are most likely a consequence of efficient cooling so that high angular momentum gas in the

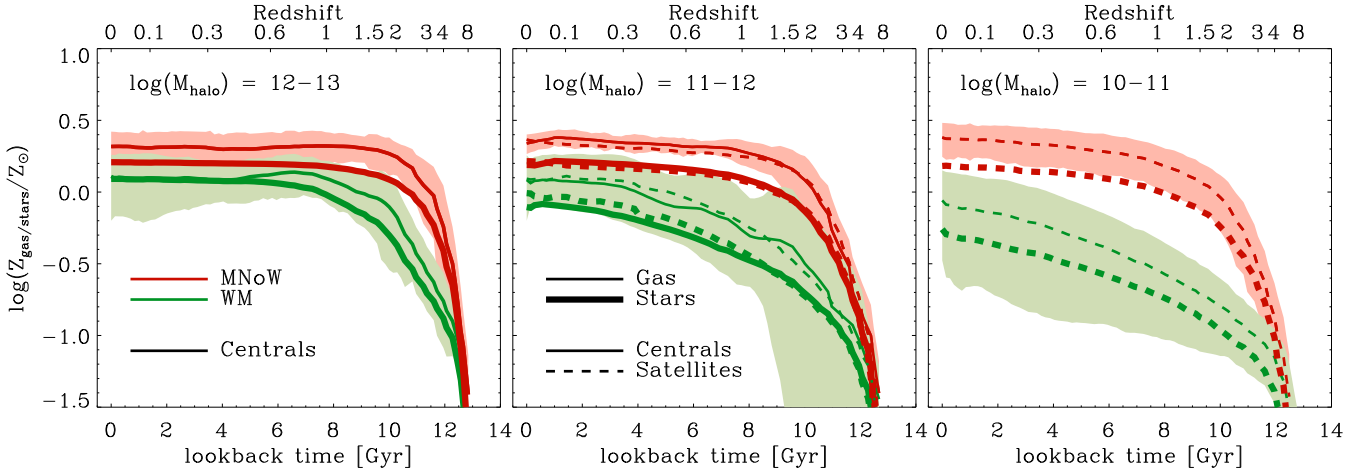


Figure 12. Time evolution of the mean gas (thin lines) and stellar metallicity (thick lines) in different halo mass bins (different panels) and distinguishing between centrals (solid lines) and satellites (dashed lines). Different colours correspond to the MNoW (red) and WM (green) model. The shaded areas show the $1\text{-}\sigma$ scatter of the mean gas metallicity, the $1\text{-}\sigma$ scatter of the mean stellar metallicity is not shown explicitly, but is similar to the gas. In the WM runs gas and stars in the galaxies are less metal-enriched than in the MNoW runs and additionally, momentum-driven winds delay the metal enrichment of both the gaseous and the stellar phase, this effect increases with decreasing halo mass.

outer parts of a galaxy can already form stars. The even larger sizes in the WM model indicate that a strong wind feedback helps to transform smaller bulge-dominated into larger disk-dominated galaxies preferentially removing low angular momentum gas. The importance of strong winds in removing low angular momentum gas was first described by Binney et al. (2001) and later discussed e.g. in Brook et al. (2011).

The top panel of Fig. 10 shows the mean half-mass radii versus redshift for massive central galaxies at $z = 0$ with $M_{\text{stellar}} > 10^{11} M_{\odot}$ and their progenitors (filled circles) as well as for lower mass centrals with $3 \times 10^{10} < M_{\text{stellar}} < 10^{11} M_{\odot}$ (open circles). For the NoMW model, the size evolution is similarly strong for high and low mass galaxies with $R_{1/2} \propto (1+z)^{\alpha}$ with $\alpha \sim -1.8$ (see also Oser et al. 2012) and the high mass galaxies are about a factor ~ 2 larger by $z = 0$. In contrast, the size evolution of the WM galaxies is much weaker ($R_{1/2} \propto (1+z)^{\alpha}$ with $\alpha = -0.9$) and there is almost no size difference between the two mass bins (see Fig. 9). The similarity to the MNoW model indicates that more efficient cooling (due to metals) without any additional galactic winds already significantly reduces the cosmological size evolution.

Inspired by van Dokkum & et al. (2013) we show the galaxy size as a function of stellar mass for high-mass (open circles) and low-mass (filled circles) progenitors at different redshifts in the bottom panel of Fig. 10. Again, NoMW galaxies evolve rapidly $R_{1/2} \sim M_{\text{stellar}}^2$ similar to observed massive galaxies (blue line) but much steeper than observed lower mass Milky-Way progenitors (green line) (van Dokkum & et al. 2013; Patel et al. 2013). In contrast, the WM model again reveals a weaker size growth as a function of mass with $R_{1/2} \sim M_{\text{stellar}}^{0.4}$ almost independent of mass and being in rough agreement with the observational trend. Compared to the recent observations of van Dokkum & et al. (2013) and Patel et al. (2013) (dotted

green and blue lines), we find that NoMW model provides a good fit to the evolution of only massive galaxies whereas the MW galaxies fit observed low mass galaxies. This is demonstrates one of our major results in this work: none of the models can reproduce the size evolution for both mass ranges at the same time. The failure of the WM model to predict a steep size evolution of massive galaxies is most likely due to their reduced fraction of accreted stellar mass and their high in situ fractions at all times and we may speculate that an additional AGN feedback may resolve this mismatch.

Fig. 11 shows the relation between the circular velocity of a galaxy and its stellar mass (Tully-Fisher relation, Tully & Fisher 1977) for the different models at $z = 0, 1, 2$. Galaxies are separated into star-forming (full colors) and quiescent (light colors) galaxies. We assume the maximum circular velocity v_{max} within r_{10} and compare to observed relations from Bell & de Jong (2001); Pizagno et al. (2005); Avila-Reese et al. (2008); Cresci et al. (2009); Miller et al. (2012). The NoMW galaxies lie above the TF relation at all redshifts due to the overproduction of centrally concentrated stellar systems. MW galaxies, however, fit the observed TF at $z = 2$ and, apart from a turn-up at $\log M_* > 10.5$, at $z = 1$ and $z = 0$ pretty well. As for this model the stellar mass within a given halo is reduced (see Fig. 7), the baryons do not dominate the circular velocity profile any more. For more massive systems the unrealistically high late star formation moves that galaxies away from the relation towards $z = 0$. Our result is agreement with a previous study of McCarthy et al. (2012) who - using the GIMIC simulations with a *constant* wind model - can also reproduce the present-day Tully-Fisher at stellar masses below $\lesssim 3 \times 10^{10} M_{\odot}$ though, but obtain a similar 'kink' at higher stellar mass, i.e. too large maximum circular velocities at a given stellar mass. This demonstrates that when the simulated Tully-Fisher relation is in agreement with the observations (high redshifts and lower mass galaxies at lower redshifts), the simulations

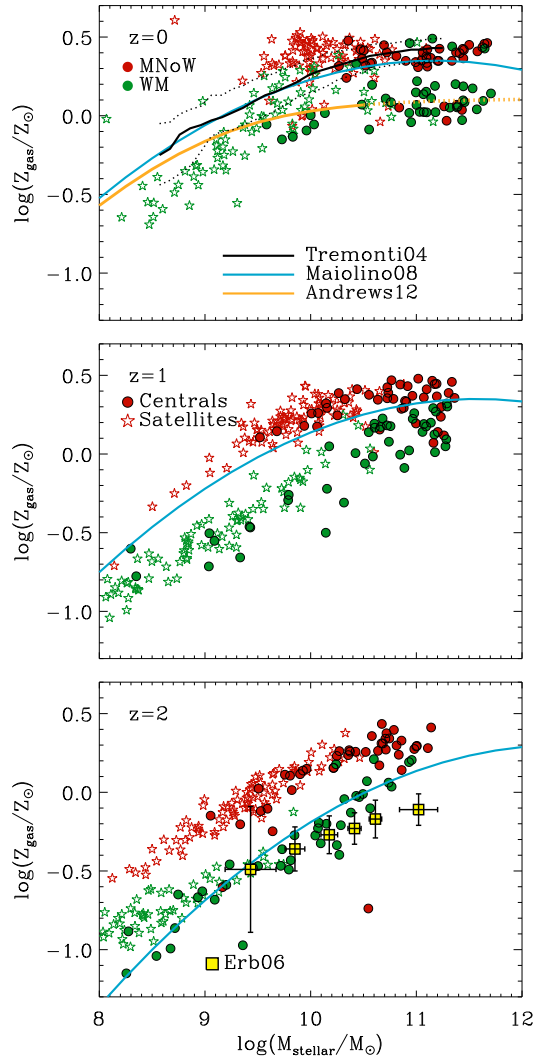


Figure 13. Gas-phase metallicity versus galaxy mass at $z = 0, 1, 2$ (from top to bottom) for the two models including metal enrichment (red, green). Filled circles and open stars indicate central and satellite galaxies, respectively. Yellow squares and solid lines illustrate measurements from Andrews & Martini (2012); Maiolino et al. (2008); Erb et al. (2006); Tremonti et al. (2004). WM runs reproduce the observational data best at $z = 2$ and the observational data of Andrews & Martini (2012) at $z = 0$, while the MNoW runs are in good agreement with observations of Tremonti et al. (2004); Maiolino et al. (2008) at $z = 0$.

also match the predictions from the abundance matching models. At low redshifts and for massive galaxies, the models are not in agreement with both the observed TF relation and the abundance matching models anymore (e.g. baryon conversion efficiencies). This result might contribute to the reliability of the abundance matching models.

6 AGES AND METALLICITY

Finally, we turn to the stellar and gas metallicity content of the simulated galaxies. Fig. 12 shows the time evolution of the mean metallicity in the gas weighted by the SFR (thin

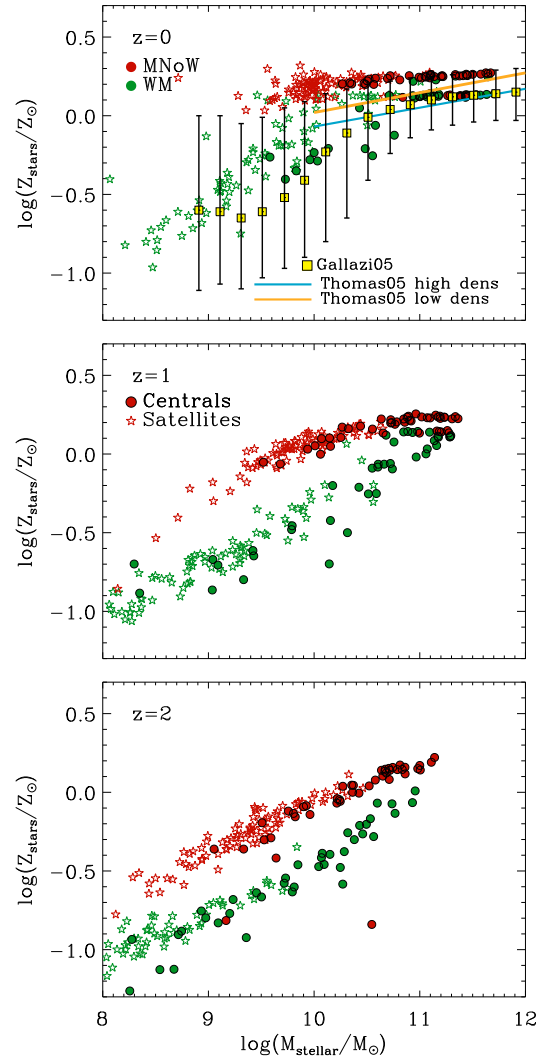


Figure 14. Same as Fig. 13, but for stellar metallicity. Yellow squares and solid lines show observational data from Thomas et al. (2005); Gallazzi et al. (2005) at $z=0$. WM runs are in good agreement with the observations. In particular the WM model reproduces the rapid decline in metallicity at masses $< 10^{11} M_{\odot}$.

lines) and the stellar component weighted by stellar mass (thick lines) within r_{10} , respectively, again binned into three different halo mass bins and distinguishing between centrals and satellites (solid and dashed lines, respectively). The $1-\sigma$ -scatter is indicated by the shaded areas, the one of the stellar metallicities is not explicitly shown, but is similar to the one of the gas metallicity. Overall, the gas metallicities are slightly higher than the stellar metallicities at a given time and halo mass as the gas gets continuously enriched. The WM runs predict more metal poor (in the gaseous and stellar phase) galaxies than the MNoW runs for the entire redshift and mass range. This is a natural consequence of the galactic winds blowing metal-enriched gas out. As an indirect consequence of the blown-out metal-rich gas, the stellar metallicity will be also reduced, since stars form out of the gas present in the centre of a galaxy (Scannapieco et al. 2006; Wiersma et al. 2009, 2011; Tissera et al. 2012, 2013).

The observed and simulated stellar and gas metallicities as a function of galaxy mass are compared in Figs. 13 and 14. Black and coloured lines and the yellow symbols illustrate different observational data from Tremonti et al. (2004); Erb et al. (2006); Maiolino et al. (2008); Andrews & Martini (2012); Thomas et al. (2005) and Gallazzi et al. (2005). Both simulation sets can reproduce a tight correlation of both the stellar and gas-phase metallicities with galaxy mass at all redshifts. The gas and stellar metallicities in the MNoW runs are found to be always larger than the ones predicted by the WM runs for the same reason as discussed above. At $z = 2$, the gas metallicities in the WM runs match the observational data well, while the MNoW runs over-predict the gas metallicity for a given galaxy mass. However, at $z = 0$ the situation is not clear as observations can differ significantly depending on the calibration method (direct mass-metallicity approach in Andrews & Martini 2012 versus the strong line calibration mass-metallicity in Tremonti et al. 2004). The gas metallicities in the MNoW runs provide a fair match to the observational data of Tremonti et al. (2004) and Maiolino et al. (2008), while the ones from WM runs agree better with the overall lower gas-phase metallicities from the study of Andrews & Martini (2012). The lower gas metallicities in the WM than in the MNoW runs may be caused by mixing of metal-enriched gas with re-infalling metal-poor gas (in the WM runs) which was blown out of the galaxy at earlier times. The stellar metallicities predicted by the WM runs agree very well with the observational data, in particular with respect to the observed decline in metallicity towards the low mass end. We want to point out that the momentum-driven wind model and the corresponding scaling of the mass loading with the velocity dispersion is *essential* for the reproduction of the steep decline in both the stellar and gas metallicity towards the low stellar mass end. Finlator & Davé (2008) and Davé et al. (2011) have demonstrated that adopting a constant wind model, i.e. with a fixed mass loading and wind velocity, produces an almost flat mass-metallicity relation with a large scatter and is, thus, in strong disagreement with observations.

We compare the mass-weighted ages to observational data in Fig. 15 for $z = 0, 1, 2$ (different panels). The MNoW runs produce a positive correlation between stellar age and galaxy mass (more massive galaxies are older) at all redshifts, but with a large scatter in the stellar age. In contrast, at $z = 1$ and $z = 2$, the WM runs produce stellar populations with ages being nearly independent of galaxy mass and also having a large scatter. At the high mass end, the stellar populations from the WM runs tend to be younger, while at the low mass end they seem to be older than the ones from the MNoW runs. The latter point is most likely due to the strong stellar feedback which prevents star formation in low-mass galaxies so that they are older. At present, the stellar ages predicted by the WM runs are also related to the galaxy mass (with a large scatter in the ages). But compared to the MNoW runs, the stellar populations of the WM runs tend to be slightly younger what is most likely a consequence increased late in situ star formation in massive galaxies compared to the MNoW runs. However, both simulation sets produce stellar populations with reasonable ages and thus, provide a fairly good match with the observed

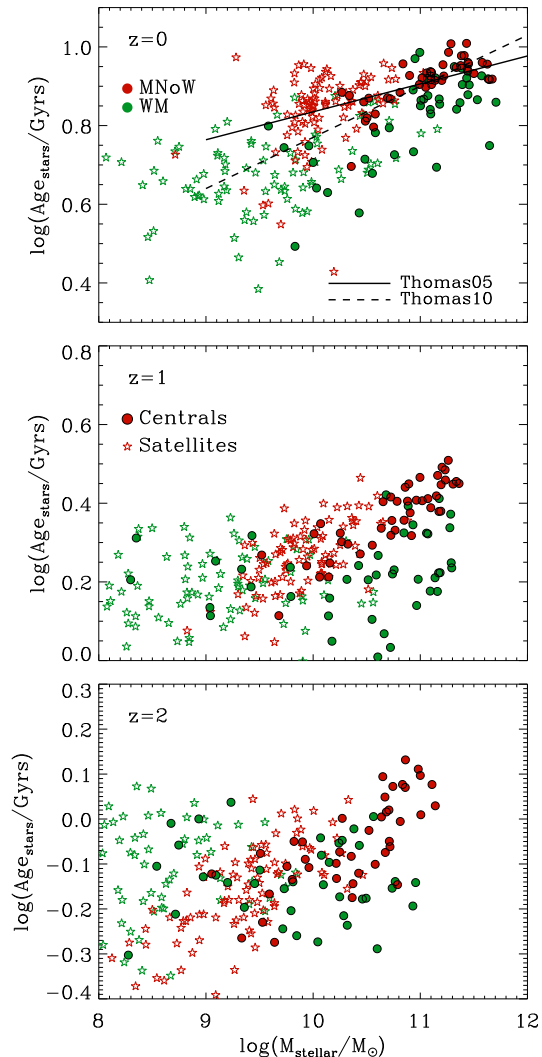


Figure 15. Average mass-weighted stellar ages for the simulated central (circles) and satellite (crosses) galaxies as a function of stellar mass. Black lines indicate observed relations from Thomas et al. (2005, 2010). The WM runs predict slightly younger galaxies than the MNoW runs, but both sets are in fairly good agreement with the observational data. At the high mass end the WM galaxies are consistently younger than observed because of the still on-going star formation at low redshifts.

stellar age-mass relations (black lines) from Thomas et al. (2005) and Thomas et al. (2010).

7 SUMMARY AND CONCLUSION

For this study, we have performed three sets of cosmological, hydrodynamical zoom simulations of 45 halos with masses between $10^{11} < M_{\text{halo}} < 10^{13} M_{\odot}$ using a modified Gadget2 version including metal enrichment and an empirical model for momentum driven galactic winds based on Oppenheimer & Davé (2006, 2008). We separately (and differentially) study the effects of metal enrichment/cooling and galactic winds on star formation, cold gas fractions, assembly histories, size evolution, metallicities and kinematic

scaling relations of the central and satellite galaxies. The main results can be summarised as follows:

(i) Galactic winds can efficiently suppress early star formation in low and high mass galaxies as the gas inflow is delayed and gas is prevented to form stars by temporarily being blown out of the galaxies. This leads to an overall increase of cold gas fractions and to a reduction of the baryon conversion efficiencies (for all halos at high redshifts and, in particular, for low mass halos at low redshift). For galaxies in massive halos $M_{\text{halo}} > 10^{12} M_{\odot}$ galactic winds shift the peak in the star formation rate from $z \sim 5$ to $z \sim 2$. For galaxies in lower mass halos the effect is even more dramatic shifting the peak from $z \sim 4$ to almost the present day. The resulting gas fractions, star formation rates and conversion efficiencies are in fairly good agreement with observations and theoretical estimates. Galactic winds provide a reasonable explanation for the observed trend that the star formation rates of low-mass galaxies peak at later cosmic times than the ones of massive galaxies (often termed as “*stellar downsizing*”), i.e. low-mass galaxies form later in time and do not necessarily follow the early formation of their low-mass halos (as predicted by a cold dark matter dominated Universe). However, the present-day mean star formation rates and baryon conversion efficiencies of our most massive galaxies are by a factor of 10 and 2-3, respectively, too large. This clearly indicates that our currently adopted wind model is not sufficient for massive galaxies, possibly due to missing AGN feedback.

(ii) Galactic winds in combination with metal enrichment lead to an increasing importance of in situ star formation over stellar accretion for the stellar mass assembly over the entire redshift range. This is caused by more efficient metal cooling (more in situ star formation) and the lower galaxy masses in accreted satellite halos (less accretion of stars). The trend for in situ fractions to increase towards lower galaxy masses is in qualitative agreement with the estimates from abundance matching models (Moster et al. 2013; Behroozi et al. 2013; Yang et al. 2013). Quantitatively, however, the WM models still predict too low in situ-to-accreted fractions for halos with masses below $M_{\text{halo}} < 10^{12} M_{\odot}$. This is most likely due to a too large amount of accreted stellar systems, which could be suppressed by a more efficient feedback for low-mass galaxies (e.g. Davé et al. 2013).

(iii) Models with galactic winds under-estimate the sizes (effective radii) of present-day massive, quiescent galaxies ($M_{\text{stellar}} > 10^{11} M_{\odot}$) as a consequence of the reduced fraction of accreted stellar systems and a too high in situ star formation at low redshifts. Models which additionally include AGN feedback may again be able to reproduce the observed, larger sizes. In contrast, the effective radii of lower mass, star-forming galaxies are strongly increased in the WM models in reasonably good agreement with the observed evolution. This holds true also for higher redshifts with the result that the relation between stellar mass and size in the wind model tends to vanish. As a consequence, the WM model predicts a much weaker size evolution than the NoWM model which is in good, qualitative agreement for intermediate mass galaxies compared to recent observational results. Overall, one of our main results is that none of our models is able to match the size evolution for high-mass and low-mass galaxies, simultaneously.

In addition, the WM model (as opposed to models without winds) can successfully reproduce the observed relation between maximum circular velocity and stellar mass for galaxies with stellar masses below $M_{\text{stellar}} < 10^{11} M_{\odot}$ at $z = 0, 1, 2$. At higher stellar masses the maximum circular velocities tend to too large in all models again pointing towards missing processes in the models as AGN feedback.

(iv) Galactic winds in zoom simulations are also found to delay the metal enrichment (as a consequence of the delayed star formation) and thus, to reduce the metallicity content (in both the stellar and gaseous component) resulting in an overall good match with observational data up to $z = 2$.

Our simulations complement previous studies by e.g. Finlator & Davé (2008); Davé (2009); Oppenheimer et al. (2010); Davé et al. (2011) and Davé et al. (2011) (who use the same model) by achieving a significantly increased mass and spatial resolution. In addition, we extend the studies of Oser et al. (2010) and Oser et al. (2012) whose simulations are based on the same initial conditions but missing metal enrichment and strong stellar feedback.

Overall, metal enrichment and strong galactic winds (even if implemented in a very phenomenological way) are shown to be essential for producing (particularly low-mass) galaxies with many reasonable properties in excellent agreement with observations (with previous, lower resolution studies). For massive galaxies at low redshifts, however, some problems still remain: the baryon conversion efficiencies and the in situ star formation rates are too high while sizes are too small. This clearly signals one or more missing further mechanisms (e.g. AGN feedback), to suppress late in situ star formation and this way to increase the fraction of accreted stars. Due to the possibly deficient galactic feedback (where the small-scale physical processes driving the winds are not resolved) the necessity for AGN feedback might be over-estimated. However, all of the currently used, different models – either simulations or semi-analytic predictions – agree that particularly for massive, quiescent galaxies, another form of feedback is required, otherwise the well-known over-cooling problem is encountered. A plausible candidate (as it was already shown in simulations and SAMs) is feedback from AGN. The relative strength of AGN and stellar feedback is, however, still model dependent. Moreover, some of our results (e.g. the too large contribution of accreted stellar systems to the overall stellar mass assembly for low-mass halos) indeed point towards a deficient implementation of stellar feedback and they tend to indicate the need for even stronger stellar winds particularly in low-mass galaxies. This is e.g. shown in a very recent study of Davé et al. (2013) who adopt an energy-driven wind model for dwarf galaxies (where the mass loading scales with σ^{-2}). This is found to even more reduce the amount low-mass galaxies and thus, match e.g. the low-mass end of the stellar mass function better. In this paper, we have only focused on the effect of metal enrichment and galactic winds on several global properties of galaxies, but in a forthcoming paper, we additionally plan to study the *radial profiles* of different baryonic components, particularly metallicity gradients, under the influence of galactic winds and how they compare to recent observations.

ACKNOWLEDGEMENTS

MH acknowledges financial support from the European Research Council under the European Community's Seventh Framework Program (FP7/2007-2013)/ERC grant agreement n. 202781. TN acknowledges support from the DFG cluster of excellence 'Origin and Structure of the Universe'. Computer resources for this project have been provided by the Leibniz Supercomputing Centre under the grant nr. pr32re. We thank the referee, Fabio Governato, for a careful and constructive reading of our paper.

REFERENCES

- Abadi M. G., Moore B., Bower R. G., 1999, *MNRAS*, 308, 947
- Abadi M. G., Navarro J. F., Steinmetz M., Eke V. R., 2003, *ApJ*, 597, 21
- Agertz O., Kravtsov A. V., Leitner S. N., Gnedin N. Y., 2013, *ApJ*, 770, 25
- Andrews B. H., Martini P., 2012, *ArXiv e-prints*
- Anglés-Alcázar D., Davé R., Özel F., Oppenheimer B. D., 2013, *ArXiv e-prints*
- Aumer M., White S. D. M., Naab T., Scannapieco C., 2013, *MNRAS*, 434, 3142
- Avila-Reese V., Zavala J., Firmani C., Hernández-Toledo H. M., 2008, *AJ*, 136, 1340
- Balogh M. L., Pearce F. R., Bower R. G., Kay S. T., 2001, *MNRAS*, 326, 1228
- Barai P., Viel M., Borgani S., Tescari E., Tornatore L., Dolag K., Killedear M., Monaco P., D'Odorico V., Cristiani S., 2013, *MNRAS*, 430, 3213
- Barai P., Viel M., Murante G., Gaspari M., Borgani S., 2013, *ArXiv e-prints*
- Behroozi P. S., Wechsler R. H., Conroy C., 2013, *ApJ*, 770, 57
- Bekki K., 2009, *MNRAS*, 399, 2221
- Bell E. F., de Jong R. S., 2001, *ApJ*, 550, 212
- Binney J., Gerhard O., Silk J., 2001, *MNRAS*, 321, 471
- Booth C. M., Schaye J., 2009, *MNRAS*, 398, 53
- Bower R. G., Benson A. J., Crain R. A., 2012, *MNRAS*, 422, 2816
- Bower R. G., Benson A. J., Malbon R., Helly J. C., Frenk C. S., Baugh C. M., Cole S., Lacey C. G., 2006, *MNRAS*, 370, 645
- Bower R. G., McCarthy I. G., Benson A. J., 2008, *MNRAS*, 390, 1399
- Brook C. B., Governato F., Roškar R., Stinson G., Brooks A. M., Wadsley J., Quinn T., Gibson B. K., Snaith O., Pilkington K., House E., Pontzen A., 2011, *MNRAS*, 415, 1051
- Brooks A. M., Solomon A. R., Governato F., McCleary J., MacArthur L. A., Brook C. B. A., Jonsson P., Quinn T. R., Wadsley J., 2011, *ApJ*, 728, 51
- Bruzual G., Charlot S., 2003, *MNRAS*, 344, 1000
- Bryan G. L., Norman M. L., 1998, *ApJ*, 495, 80
- Cattaneo A., Dekel A., Devriendt J., Guiderdoni B., Blaizot J., 2006, *MNRAS*, 370, 1651
- Cen R., Chisari N. E., 2011, *ApJ*, 731, 11
- Cen R., Ostriker J. P., 2000, *ApJ*, 538, 83
- Ceverino D., Klypin A., 2009, *ApJ*, 695, 292
- Chabrier G., 2003, *PASP*, 115, 763
- Choi E., Ostriker J. P., Naab T., Johansson P. H., 2012, *ApJ*, 754, 125
- Ciotti L., Ostriker J. P., Proga D., 2010, *ApJ*, 717, 708
- Cresci G., Hicks E. K. S., Genzel R., Schreiber N. M. F., Davies R., Bouché N., Buschkamp P., Genel S., Shapiro K., Tacconi L., Sommer-Larsen J., 2009, *ApJ*, 697, 115
- Croton D. J., Springel V., White S. D. M., De Lucia G., Frenk C. S., Gao L., Jenkins A., Kauffmann G., Navarro J. F., Yoshida N., 2006, *MNRAS*, 365, 11
- Daddi E., Dickinson M., Morrison G., Chary R., Cimatti A., Elbaz D., Frayer D., Renzini A., Pope A., Alexander D. M., Bauer F. E., Giavalisco M., Huynh M., Kurk J., Mignoli M., 2007, *ApJ*, 670, 156
- Dalla Vecchia C., Schaye J., 2008, *MNRAS*, 387, 1431
- Dalla Vecchia C., Schaye J., 2012, *MNRAS*, 426, 140
- Davé R., 2009, in Jogee S., Marinova I., Hao L., Blanc G. A., eds, *Galaxy Evolution: Emerging Insights and Future Challenges* Vol. 419 of *Astronomical Society of the Pacific Conference Series*, Missing Halo Baryons and Galactic Outflows. p. 347
- Davé R., Finlator K., Oppenheimer B. D., 2011, *MNRAS*, 416, 1354
- Davé R., Katz N., Oppenheimer B. D., Kollmeier J. A., Weinberg D. H., 2013, *MNRAS*, 434, 2645
- Davé R., Oppenheimer B. D., Finlator K., 2011, *MNRAS*, 415, 11
- Davis M., Efstathiou G., Frenk C. S., White S. D. M., 1985, *ApJ*, 292, 371
- De Lucia G., Kauffmann G., White S. D. M., 2004, *MNRAS*, 349, 1101
- De Lucia G., Springel V., White S. D. M., Croton D., Kauffmann G., 2006, *MNRAS*, 366, 499
- Dubois Y., Gavazzi R., Peirani S., Silk J., 2013, *MNRAS*, 433, 3297
- Dutton A. A., van den Bosch F. C., Dekel A., 2010, *MNRAS*, 405, 1690
- Elbaz D., Daddi E., Le Borgne D., Dickinson M., Alexander D. M., Chary R., Starck J., Brandt W. N., Kitzbichler M., MacDonald E., Nonino M., Popesso P., Stern D., Vanzella E., 2007, *A&A*, 468, 33
- Elbaz D., Dickinson M., Hwang H. S., Díaz-Santos T., Magdis G., Magnelli B., Le Borgne D., Galliano F., Pannella M., Chanial P., Armus L., Charmandaris V., 2011, *A&A*, 533, A119
- Erb D. K., Shapley A. E., Pettini M., Steidel C. C., Reddy N. A., Adelberger K. L., 2006, *ApJ*, 644, 813
- Fabjan D., Borgani S., Tornatore L., Saro A., Murante G., Dolag K., 2010, *MNRAS*, 401, 1670
- Fanidakis N., Baugh C. M., Benson A. J., Bower R. G., Cole S., Done C., Frenk C. S., 2011, *MNRAS*, 410, 53
- Finlator K., Davé R., 2008, *MNRAS*, 385, 2181
- Font A. S., Bower R. G., McCarthy I. G., Benson A. J., Frenk C. S., Helly J. C., Lacey C. G., Baugh C. M., Cole S., 2008, *MNRAS*, 389, 1619
- Forbes D. A., Ponman T., O'Sullivan E., 2012, *MNRAS*, 425, 66
- Forbes D. A., Spitler L. R., Strader J., Romanowsky A. J., Brodie J. P., Foster C., 2011, *MNRAS*, 413, 2943
- Franx M., van Dokkum P. G., Schreiber N. M. F., Wuyts S., Labbé I., Toft S., 2008, *ApJ*, 688, 770
- Gabor J. M., Davé R., 2012, *MNRAS*, 427, 1816

- Gallazzi A., Charlot S., Brinchmann J., White S. D. M., Tremonti C. A., 2005, *MNRAS*, 362, 41
- Genel S., Naab T., Genzel R., Förster Schreiber N. M., Sternberg A., Oser L., Johansson P. H., Davé R., Oppenheimer B. D., Burkert A., 2012, *ApJ*, 745, 11
- Genzel R., et al., 2010, *MNRAS*, 407, 2091
- Genzel R., Newman S., Jones T., Förster Schreiber N. M., Shapiro K., Genel S., Lilly S. J., Renzini A., Tacconi L. J., Bouché N., Burkert A., 2011, *ApJ*, 733, 101
- Governato F., Brook C., Mayer L., Brooks A., Rhee G., Wadsley J., Jonsson P., Willman B., Stinson G., Quinn T., Madau P., 2010, *Nature*, 463, 203
- Governato F., Willman B., Mayer L., Brooks A., Stinson G., Valenzuela O., Wadsley J., Quinn T., 2007, *MNRAS*, 374, 1479
- Governato F., Zolotov A., Pontzen A., Christensen C., Oh S. H., Brooks A. M., Quinn T., Shen S., Wadsley J., 2012, *MNRAS*, 422, 1231
- Gunn J. E., Gott III J. R., 1972, *ApJ*, 176, 1
- Guo Q., White S., Boylan-Kolchin M., De Lucia G., Kauffmann G., Lemson G., Li C., Springel V., Weinmann S., 2011, *MNRAS*, pp 164–+
- Guo Q., White S. D. M., 2008, *MNRAS*, 384, 2
- Haardt F., Madau P., 2001, in Neumann D. M., Tran J. T. V., eds, *Clusters of Galaxies and the High Redshift Universe Observed in X-rays Modelling the UV/X-ray cosmic background with CUBA*
- Haas M. R., Schaye J., Booth C. M., Dalla Vecchia C., Springel V., Theuns T., Wiersma R. P. C., 2012, *ArXiv e-prints*
- Hilz M., Naab T., Ostriker J. P., 2013, *MNRAS*, 429, 2924
- Hilz M., Naab T., Ostriker J. P., Thomas J., Burkert A., Jesseit R., 2012, *MNRAS*, 425, 3119
- Hirschmann M., Khochfar S., Burkert A., Naab T., Genel S., Somerville R. S., 2010, *MNRAS*, 407, 1016
- Hirschmann M., Naab T., Somerville R. S., Burkert A., Oser L., 2012, *MNRAS*, 419, 3200
- Hirschmann M., Somerville R. S., Naab T., Burkert A., 2012, *MNRAS*, 426, 237
- Hopkins P. F., Cox T. J., Hernquist L., Narayanan D., Hayward C. C., Murray N., 2013, *MNRAS*, 430, 1901
- Hopkins P. F., Hernquist L., Cox T. J., Di Matteo T., Martini P., Robertson B., Springel V., 2005, *ApJ*, 630, 705
- Hopkins P. F., Quataert E., Murray N., 2011, *MNRAS*, 417, 950
- Hopkins P. F., Quataert E., Murray N., 2012, *MNRAS*, 421, 3522
- Hummels C. B., Bryan G. L., 2012, *ApJ*, 749, 140
- Johansson P. H., Naab T., Ostriker J. P., 2009, *ApJ*, 697, L38
- Johansson P. H., Naab T., Ostriker J. P., 2012, *ApJ*, 754, 115
- Kang X., Jing Y. P., Silk J., 2006, *ApJ*, 648, 820
- Kannan R., Macciò A. V., Pasquali A., Moster B. P., Walter F., 2012, *ApJ*, 746, 10
- Katz N., Hernquist L., Weinberg D. H., 1992, *ApJ*, 399, L109
- Katz N., Weinberg D. H., Hernquist L., 1996, *ApJS*, 105, 19
- Kauffmann G., White S. D. M., Guiderdoni B., 1993, *MNRAS*, 264, 201
- Kawata D., Mulchaey J. S., 2008, *ApJ*, 672, L103
- Kereš D., Vogelsberger M., Sijacki D., Springel V., Hernquist L., 2012, *MNRAS*, 425, 2027
- Khochfar S., Silk J., 2006, *ApJ*, 648, L21
- Lackner C. N., Cen R., Ostriker J. P., Joung M. R., 2012, *MNRAS*, 425, 641
- Limongi M., Chieffi A., 2005, in Turatto M., Benetti S., Zampieri L., Shea W., eds, *1604-2004: Supernovae as Cosmological Lighthouses Vol. 342 of Astronomical Society of the Pacific Conference Series, Presupernova Evolution and Explosive Nucleosynthesis of Massive Stars at Various Metallicities from $Z=0$ to $Z = Z_{\odot}$* . p. 122
- Maiolino R., Nagao T., Grazian A., Cocchia F., Marconi A., Mannucci F., Cimatti A., Pipino A., Ballero S., Calura F., 2008, *A&A*, 488, 463
- Marinacci F., Pakmor R., Springel V., 2013, *ArXiv e-prints*
- Martin C. L., 2005, *ApJ*, 621, 227
- Martizzi D., Teyssier R., Moore B., 2012, *MNRAS*, 420, 2859
- Maulbetsch C., Avila-Reese V., Colín P., Gottlöber S., Khalatyan A., Steinmetz M., 2007, *ApJ*, 654, 53
- McCarthy I. G., Frenk C. S., Font A. S., Lacey C. G., Bower R. G., Mitchell N. L., Balogh M. L., Theuns T., 2008, *MNRAS*, 383, 593
- McCarthy I. G., Schaye J., Font A. S., Theuns T., Frenk C. S., Crain R. A., Dalla Vecchia C., 2012, *MNRAS*, 427, 379
- McCarthy I. G., Schaye J., Ponman T. J., Bower R. G., Booth C. M., Dalla Vecchia C., Crain R. A., Springel V., Theuns T., Wiersma R. P. C., 2010, *MNRAS*, 406, 822
- McKee C. F., Ostriker J. P., 1977, *ApJ*, 218, 148
- Miller S. H., Ellis R. S., Sullivan M., Bundy K., Newman A. B., Treu T., 2012, *ApJ*, 753, 74
- Monaco P., Fontanot F., Taffoni G., 2007, *MNRAS*, 375, 1189
- Moster B. P., Naab T., White S. D. M., 2013, *MNRAS*, 428, 3121
- Moster B. P., Somerville R. S., Maulbetsch C., van den Bosch F. C., Macciò A. V., Naab T., Oser L., 2010, *ApJ*, 710, 903
- Munshi F., Governato F., Brooks A. M., Christensen C., Shen S., Loebman S., Moster B., Quinn T., Wadsley J., 2013, *ApJ*, 766, 56
- Murante G., Monaco P., Giovalli M., Borgani S., Diaferio A., 2010, *MNRAS*, 405, 1491
- Murray N., Quataert E., Thompson T. A., 2005, *ApJ*, 618, 569
- Naab T., Johansson P. H., Ostriker J. P., 2009, *ApJ*, 699, L178
- Naab T., Johansson P. H., Ostriker J. P., Efstathiou G., 2007, *ApJ*, 658, 710
- Navarro J. F., White S. D. M., 1993, *MNRAS*, 265, 271
- Neistein E., van den Bosch F. C., Dekel A., 2006, *MNRAS*, 372, 933
- Newman S. F., Genzel R., Förster-Schreiber N., Shapiro Griffin K., Mancini C., Lilly S. J., 2012, *ArXiv e-prints*
- Nipoti C., Treu T., Auger M. W., Bolton A. S., 2009, *ApJ*, 706, L86
- Noeske K. G., Weiner B. J., Faber S. M., Papovich C., Koo D. C., Somerville R. S., Bundy K., Conselice C. J., Newman J. A., Schiminovich D., Le Floch E., 2007, *ApJ*, 660, L43
- Oppenheimer B. D., Davé R., 2006, *MNRAS*, 373, 1265

- Oppenheimer B. D., Davé R., 2008, *MNRAS*, 387, 577
- Oppenheimer B. D., Davé R., Finlator K., 2009, *MNRAS*, 396, 729
- Oppenheimer B. D., Davé R., Kereš D., Fardal M., Katz N., Kollmeier J. A., Weinberg D. H., 2010, *MNRAS*, 406, 2325
- Oser L., Naab T., Ostriker J. P., Johansson P. H., 2012, *ApJ*, 744, 63
- Oser L., Ostriker J. P., Naab T., Johansson P. H., Burkert A., 2010, *ApJ*, 725, 2312
- Patel S. G., van Dokkum P. G., Franx M., Quadri R. F., Muzzin A., Marchesini D., Williams R. J., Holden B. P., Stefanon M., 2013, *ApJ*, 766, 15
- Peeples M. S., Shankar F., 2011, *MNRAS*, 417, 2962
- Piontek F., Steinmetz M., 2011, *MNRAS*, 410, 2625
- Pizagno J., Prada F., Weinberg D. H., Rix H.-W., Harbeck D., Grebel E. K., Bell E. F., Brinkmann J., Holtzman J., West A., 2005, *ApJ*, 633, 844
- Porter L. A., Somerville R. S., Croton D. J., Covington M. D., Graves G. J., Faber S. M., Primack J. R., 2012, *ArXiv e-prints*
- Puchwein E., Sijacki D., Springel V., 2008, *ApJ*, 687, L53
- Puchwein E., Springel V., 2012, *ArXiv e-prints*
- Puchwein E., Springel V., 2013, *MNRAS*, 428, 2966
- Quilis V., Moore B., Bower R., 2000, *Science*, 288, 1617
- Reddy N. A., Pettini M., Steidel C. C., Shapley A. E., Erb D. K., Law D. R., 2012, *ApJ*, 754, 25
- Rees M. J., Ostriker J. P., 1977, *MNRAS*, 179, 541
- Roediger E., Brüggem M., 2007, *MNRAS*, 380, 1399
- Rupke D. S., Veilleux S., Sanders D. B., 2005, *ApJS*, 160, 115
- Saintonge A., Kauffmann G., Kramer C., Tacconi L. J., Buchbender C., Catinella B., Fabello S., Graciá-Carpio J., Wang J., Cortese L., Fu J., Genzel R., 2011, *MNRAS*, 415, 32
- Salim S., Rich R. M., Charlot S., Brinchmann J., Johnson B. D., Schiminovich D., Seibert M., Mallery R., Heckman T. M., Forster K., Friedmann P. G., 2007, *ApJS*, 173, 267
- Sawala T., Guo Q., Scannapieco C., Jenkins A., White S., 2011, *MNRAS*, 413, 659
- Scannapieco C., Tissera P. B., White S. D. M., Springel V., 2006, *MNRAS*, 371, 1125
- Scannapieco C. e. a., 2012, *MNRAS*, 423, 1726
- Scannapieco E., Bildsten L., 2005, *ApJ*, 629, L85
- Schaye J., Dalla Vecchia C., Booth C. M., Wiersma R. P. C., Theuns T., Haas M. R., Bertone S., Duffy A. R., McCarthy I. G., van de Voort F., 2010, *MNRAS*, 402, 1536
- Shen S., Mo H. J., White S. D. M., Blanton M. R., Kauffmann G., Voges W., Brinkmann J., Csabai I., 2003, *MNRAS*, 343, 978
- Sijacki D., Springel V., Di Matteo T., Hernquist L., 2007, *MNRAS*, 380, 877
- Sijacki D., Vogelsberger M., Kereš D., Springel V., Hernquist L., 2012, *MNRAS*, 424, 2999
- Somerville R. S., Hopkins P. F., Cox T. J., Robertson B. E., Hernquist L., 2008, *MNRAS*, 391, 481
- Spergel D. N., Verde L., Peiris H. V., Komatsu E., Nolte M. R., Bennett C. L., Halpern M., Hinshaw G., Jarosik N., Kogut A., Limon M., Meyer S. S., Page L., Tucker G. S., Weiland J. L., Wollack E., Wright E. L., 2003, *ApJS*, 148, 175
- Springel V., 2010, *MNRAS*, 401, 791
- Springel V., Di Matteo T., Hernquist L., 2005, *MNRAS*, 361, 776
- Springel V., Hernquist L., 2003, *MNRAS*, 339, 289
- Springel V., White S. D. M., Jenkins A., Frenk C. S., Yoshida N., Gao L., Navarro J., Thacker R., Croton D., Helly J., Peacock J. A., Cole S., Thomas P., Couchman H., Evrard A., Colberg J., Pearce F., 2005, *Nature*, 435, 629
- Springel V., Yoshida N., White S. D. M., 2001, *New Astronomy*, 6, 79
- Steidel C. C., Erb D. K., Shapley A. E., Pettini M., Reddy N., Bogosavljević M., Rudie G. C., Rakic O., 2010, *ApJ*, 717, 289
- Steinmetz M., Muller E., 1995, *MNRAS*, 276, 549
- Stinson G., Seth A., Katz N., Wadsley J., Governato F., Quinn T., 2006, *MNRAS*, 373, 1074
- Stinson G. S., Brook C., Macciò A. V., Wadsley J., Quinn T. R., Couchman H. M. P., 2012, *MNRAS*, p. 18
- Stinson G. S., Brook C., Macciò A. V., Wadsley J., Quinn T. R., Couchman H. M. P., 2013, *MNRAS*, 428, 129
- Sutherland R. S., Dopita M. A., 1993, *ApJS*, 88, 253
- Tacconi L. J., et al. 2013, *ApJ*, 768, 74
- Tacconi L. J., Genzel R., Neri R., Cox P., Cooper M. C., Shapiro K., Bolatto A., Bouché N., Bournaud F., Burkert A., 2010, *Nature*, 463, 781
- Teyssier R., Moore B., Martizzi D., Dubois Y., Mayer L., 2011, *MNRAS*, 414, 195
- Thomas D., Maraston C., Bender R., Mendes de Oliveira C., 2005, *ApJ*, 621, 673
- Thomas D., Maraston C., Schawinski K., Sarzi M., Silk J., 2010, *MNRAS*, 404, 1775
- Tissera P. B., Scannapieco C., Beers T. C., Carollo D., 2013, *MNRAS*, 432, 3391
- Tissera P. B., White S. D. M., Scannapieco C., 2012, *MNRAS*, 420, 255
- Tremonti C. A., Heckman T. M., Kauffmann G., Brinchmann J., Charlot S., White S. D. M., Seibert M., Peng E. W., Schlegel D. J., Uomoto A., Fukugita M., Brinkmann J., 2004, *ApJ*, 613, 898
- Tully R. B., Fisher J. R., 1977, *A&A*, 54, 661
- van de Voort F., Schaye J., Booth C. M., Dalla Vecchia C., 2011, *MNRAS*, 415, 2782
- van Dokkum P. G., et al. 2013, *ApJ*, 771, L35
- van Gorkom J. H., 2004, *Clusters of Galaxies: Probes of Cosmological Structure and Galaxy Evolution*, p. 305
- Vogelsberger M., Genel S., Sijacki D., Torrey P., Springel V., Hernquist L., 2013, *ArXiv e-prints*
- Wake D. A., Whitaker K. E., Labbé I., van Dokkum P. G., Franx M., Quadri R., Brammer G., Kriek M., Lundgren B. F., Marchesini D., Muzzin A., 2011, *ApJ*, 728, 46
- Weiner B. J., Coil A. L., Prochaska J. X., Newman J. A., Cooper M. C., Bundy K., Conselice C. J., Dutton A. A., Faber S. M., Koo D. C., Lotz J. M., Rieke G. H., Rubin K. H. R., 2009, *ApJ*, 692, 187
- Weinmann S. M., Pasquali A., Oppenheimer B. D., Finlator K., Mendel J. T., Crain R. A., Macciò A. V., 2012, *MNRAS*, 426, 2797
- White S. D. M., Frenk C. S., 1991, *ApJ*, 379, 52
- White S. D. M., Rees M. J., 1978, *MNRAS*, 183, 341
- Wiersma R. P. C., Schaye J., Theuns T., 2011, *MNRAS*, 415, 353

Wiersma R. P. C., Schaye J., Theuns T., Dalla Vecchia C., Tornatore L., 2009, MNRAS, 399, 574
 Williams R. J., Quadri R. F., Franx M., van Dokkum P., Toft S., Kriek M., Labbé I., 2010, ApJ, 713, 738
 Yang X., Mo H. J., van den Bosch F. C., Bonaca A., Li S., Lu Y., Lu Y., Lu Z., 2013, ArXiv e-prints
 Zhang D., Thompson T. A., 2012, MNRAS, 424, 1170

APPENDIX A: EFFECTS OF NUMERICAL RESOLUTION

For one high- and low-mass halo with final masses of $M_{\text{halo}} \sim 10^{12} M_{\odot}$ (M0977) and $M_{\text{halo}} \sim 2 \times 10^{11} M_{\odot}$ (M6782) we have performed re-simulations including metal cooling and winds with a *four* times better spatial resolution (i.e. reduced softening length by a factor of four, i.e. 4x-resimulations) than the original one to study the convergence of our results with higher resolution. As for the 2x-resolution runs, we traced back the particles that are closer than $2 \times r_{200}$ to the centre of the halo in any of our snapshots in the original DM-only simulation ($m_{\text{dm}} = 2 \times 10^8 M_{\odot} h^{-1}$) and replace them with dark matter and gas particles of higher resolution, achieving a 64 times better mass resolution in the high-resolution region than in the original DM simulation (and thus, an eight times better mass resolution than the 2x-resimulations which are considered throughout this work): $m_{\text{dm}} = 3.1 \times 10^6 M_{\odot} h^{-1}$ and $m_{\text{gas}} = m_{\text{star}} = 5.3 \times 10^5 M_{\odot} h^{-1}$.

As shown in the upper left panel of Fig A The mass aggregation history of the dark matter component in both haloes (pink and turquoise lines) is very similar for the two different resolution limits (4x-resolution: solid lines and 2x-resolution: dashed lines). This also suggests that the haloes with different resolution have experienced the same amount major/minor mergers. Regarding the baryons, we show in Fig. A the evolution of the stellar mass, the cold gas fractions and the SFRs of the central galaxy. We find that the haloes with four times larger spatial resolution contain slightly more massive galaxies with slightly smaller cold gas fractions, but higher SFRs. This indicates that with increasing resolution the wind feedback seems to become very slightly less efficient. This is only a weak effect, which we have already mentioned before in order to explain the small differences between our 2x-resimulations and the results from previous studies using the same code but having a worse resolution (Oppenheimer & Davé 2006, 2008; Davé 2009; Davé et al. 2011). To summarise, we find no significant difference in the evolution of the central galaxy/main halo in the simulations with different resolution. Therefore, due to computational costs, we restrict our main study to 2x-resimulations (i.e. the dashed lines in Fig. A).

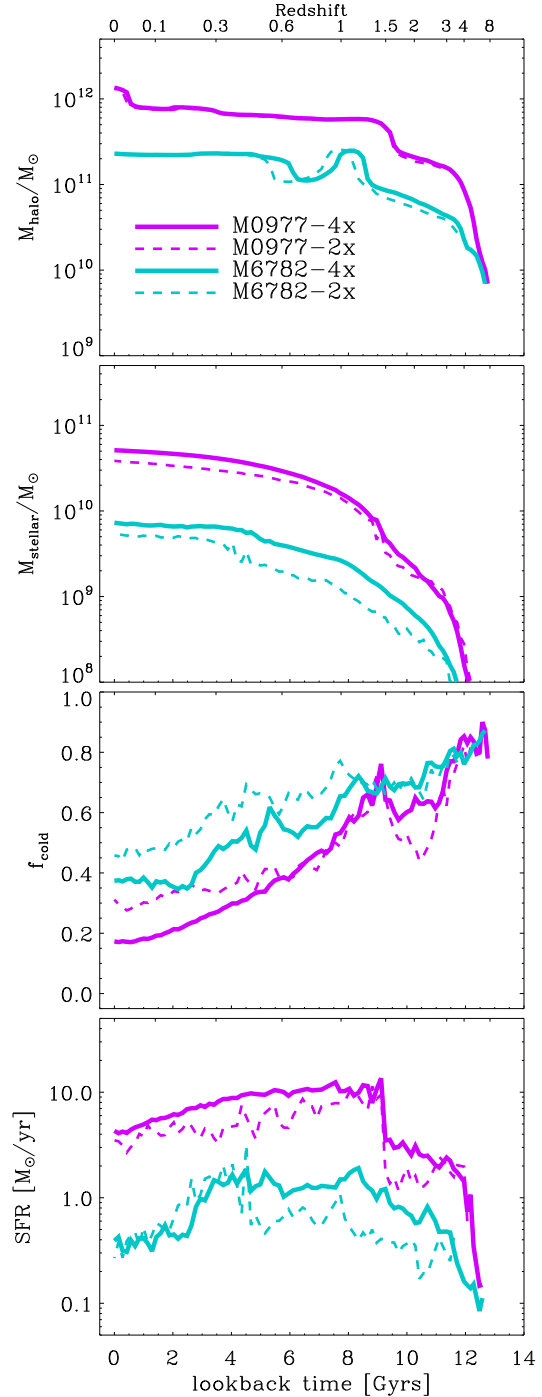


Figure A1. Cosmic evolution of halo mass, stellar mass, cold gas fractions and SFRs for two different haloes (M0977: $M_{\text{halo}} \sim 10^{12} M_{\odot}$, pink lines and M6782: $M_{\text{halo}} \sim 2 \times 10^{11} M_{\odot}$ turquoise lines) with 2x (dashed lines) and 4x (solid lines) resolution. We find no significant difference in the evolution of the central galaxy/main halo in the corresponding runs with different resolution.